Developing Paper-Based Microfluidics for the CRISPR Diagnostic of Infectious Diseases

BY

AUJCHARA THEPBUT 63011113

A PROJECT SUBMITTED IN PARTIAL FULFILLMENT OF THE REQUIREMENTS FOR THE DEGREE OF BACHELOR OF ENGINEERING IN BIOMEDICAL ENGINEERING
KING MONGKUT'S INSTITUTE OF TECHNOLOGY LADKRABANG
ACADEMIC YEAR 2023

SCHOOL OF ENGINEERING

KING MONGKUT'S INSTITUTE OF TECHNOLOGY LADKRABANG

PROJECT CERTIFICATE

Project Title	Developing Paper-Based Microfluidics for the CRISPR Diagnostic of Infectious Diseases
Student Name	Miss Aujchara Thepbut Student ID. 63011113
Degree	Bachelor of Engineering in Biomedical
Project Advisor	Signed: _____ (Asst. Prof. Dr. Pimkhuan Hannanta-anan)
Committee	Signed: _____ (Assoc. Prof. Dr. Matthew Paul Gleeson)
Committee	Signed: _____ (Asst. Prof. Dr. Jamie Alexander O'Reilly)
Committee	Signed: _____ (Dr. May Phu Paing)
Head of Department	Signed: _____ (Assoc. Prof. Dr. Sarinporn Visitsattapongse)

Project Title	Developing Paper-Based Microfluidics for the CRISPR Diagnostic of Infectious Diseases
Student Name	Miss Aujchara Thepbut Student ID. 63011113
Degree	Bachelor of Engineering in Biomedical Engineering
Project Advisor	Asst. Prof. Pimkhuan Hannanta-anan
Academic Years	2023

ABSTRACT

Since December 2019, a Coronavirus Disease (COVID-19) has spread and infected from person-to-person across the world. It is an infectious disease, caused by the SAR-CoV-2 virus. Currently, the gold standard for COVID-19 detection is RT-PCR. However, RT-PCR is expensive and time-consuming. An alternative such as the ATK method can reduce the detection time and increase ease of use, but the sensitivity of this method is only 49%. The CRISPR-Cas12a system is developed to be a novel detection method, which provides a high sensitivity and specificity rivaling RT-PCR while sharing the ease of use and rapidity of test of the ATK method. This project aims to apply the CRISPR-Cas12a system into the paper-based microfluidic devices by integrating the multiple steps of assay within one device for creating a novel diagnostic platform owing to increase the accessibility, high accuracy, provides a rapid testing, low-cost point-of-care (POC) medical diagnostics, high biocompatibility, and easy to fabricate. This project commenced with the assumption of sufficient target sequences of DNA template in the sample, eliminating the requirements of amplification step (30 minutes) and only focused on the Cas12a detection step (15 minutes).

The device's designs were created via AutoCAD 2023 program and easily fabricated hydrophobic barriers on Double Ring 102 filter paper by Thermal Transfer Printer. The devices were heated to melt the carbon ribbon by using an electric oven for 15 minutes at 120 °C, which is the optimal heating temperature and heating time. In order to analyze the effective of sample mixing in microchannel, three different designs of prototype i.e., cross-shape, T-shape, and Y-shape, were utilized with yellow and blue dye solutions representing as samples and CRISPR reagents, forming green color. This colorimetric analysis used the Hue from HSV color model to analyze the sample mixing in microchannel. The results indicated that the cross-shape is the most effective design for liquid mixing as we observed 80% sample mixing at a shorter distance than other designs. The optimal characteristic of devices is 4 mm in channel width and 2.55 mm in channel length. Additionally, the optimal sample and CRISPR reagent volume is 40 μL. In conclusion, we successfully created paper-based microfluidic devices with an optimal design for regulating the flows and the mixing of the CRISPR-Cas12a system.

ACKNOWLEDGEMENTS

First and foremost, I would like to express my deepest and sincere gratitude to my project advisor, Asst. Prof. Pimkhuan Hannanta-anan, for giving me the opportunity to conduct this research and for her invaluable advice throughout this semester. I have been greatly inspired by her drive, vision, sincerity, and motivation. She has taught me how to conduct the research and to convey the outcomes as clearly as possible. Being to work and study under her guidance was a great honor.

I am extremely grateful to my parents for their unwavering support, love, and encouragement throughout this project. Without their support and motivations, this thesis would not have been possible to finish as my expectations. Finally, I would like to thank all of professors in Biomedical Engineering Department at King Mongkut's Institute of Technology Ladkrabang for their teaching and guidance throughout my academic journey and contributed significantly to my personal growth and development.

Aujchara Thepbut

TABLE OF CONTENTS

LIST OF TABLES

LIST OF FIGURES

LIST OF SYMBOLS/ABBREVIATIONS

Symbols/Abbreviations	Terms
ACE2 receptor	Angiotensin Converting Enzyme 2 receptor
ARDS	Acute Respiratory Distress Syndrome
ATK	Antigen Test Kit
COVID-19	Coronavirus Disease 2019
CRISPR	Clustered Regularly Interspaced Short Palindromic Repeats
crRNA	CRISPR RNA
DETECTR	DNA Endonuclease-Targeted CRISPR Trans Reporter
DMVs	The double-membrane vesicles
DNA	Deoxyribonucleic Acid
E protein	Envelop protein
ER	Endoplasmic Reticulum
FDA	Food and Drug Administration
LFAs	Lateral Flow Assays
LOC	Lab-On-Chip
M protein	Membrane protein
N protein	Nucleocapsid
NSPs	The individual non-structural protein
ORF	Open Reading Frames
POC	Point-Of-Care
Pp1a	Polyprotein 1 a
Pp1ab	Polyprotein 1 ab
RNA	Ribonucleic Acid
RT-PCR	Reverse Transcription Polymerase Chain Reaction
RT-qPCR	Reverse Transcription Quantitative

	Polymerase Chain Reaction
S protein	Spike protein
SARS-CoV-2	Severe Acute Respiratory Syndrome-Coronavirus-2
WHO	The World Health Organization

CHAPTER 1

INTRODUCTION

1.1 Background and significance of the study

Since December 2019, a Coronavirus Disease (COVID-19) was first reported in Wuhan, China [1]. It is an infectious disease, caused by the SARS-CoV-2 virus, that has spread and infected from person-to-person across the world. The symptoms that commonly observe in COVID-19 patients are high fever, cough, sore throat, headache, and difficulty breathe, which likely influenza. However, in the severe cases can be found with acute respiratory distress syndrome (ARDS), which become a serious illness or death [2]. In these 3 years, 4.4 million Thailand people were infected by COVID-19 and number of deaths were continuous increased to approximately 30,000 people [3].

Currently, the diagnostic method, which is the gold standard protocol, for detection COVID-19 is Real-time reverse transcription polymerase chain reaction (Real-Time RT-PCR). However, RT-PCR is expensive, require only special technicians to perform test, inappropriate for screening in a large number of people, and time-consuming, which takes time up to 24 hours. So, it had a proposal to use a Rapid test by using Antigen Test Kits instead. This advantage of ATK is it takes time to test and get the result of testing only 15 – 30 minutes, the main disadvantage of ATK is it has high false negative result, which has 11.5%, that made this method cannot be a standard diagnostic method for COVID-19 [4]. Therefore, to develop a new diagnostic method, both method of RT-PCR and Rapid Test by using ATK were selected for combining their advantages by using a paper-based microfluidic device as a platform and apply with CRISPR-Cas12-based assay for SARS-CoV-2 detection.

CRISPR-based assay is the technique that can be used to detect SARS-CoV-2 and it was approved by US Food and Drug Administration (FDA). CRISPR-Cas and recombinase polymerase amplification were combined together for target sequences of DNA amplification and detection. The specific target sequences of the DNA were

cleaved by a Cas protein, which has the matching DNA target sequences with CRISPR RNA (crRNA). After matching DNA target sequence, it activates a Cas12a to cleave the fluorescent reporter from the quencher and the fluorescent signals were illuminated. So, to apply this assay in this project, this diagnostic method is not only indicating the qualitative result, but it also indicating as a quantitative result [2].

In order to apply the CRISPR-base assay in some platforms, the paper-based microfluidic device was selected to use because this technique is assembled multiple steps of assay within one device, which provide a convenience of usage, low cost, biocompatibility, and easy to fabricate.

1.2 Objectives

To develop the paper-based microfluidic device for CRISPR diagnostic as a new diagnostic kit, which can be applied to detect an infectious disease, is the overall objective of this project. Based on this thesis project, the main objective in this semester is clarified into 2 sub aims which are:

1. To identify the most effective condition for achieving fabrication of paper-based microfluidic device by using printing technique.
2. To design a paper-based microfluidic that can regulate flow rate and liquid mixing, appropriate for facilitation the CRISPR diagnostic assay.

1.3 Hypothesis

Paper-based microfluidic device achieves to fabricate by using printing technique with the most effective condition and can be modified the characteristics of the device to apply the CRISPR-Cas12-based assay into a device to be a first protocol, which prepared for testing with the real samples and reagents in the future.

1.4 Scope of Study

The aim of this project is to develop the paper-based microfluidic device and apply the CRISPR-Cas12-based assay as a new diagnostic kit by using a Thermal Transfer Printer to fabricate the device to improve the recent diagnostic method for detection of infectious disease. To achieve the developing paper-based microfluidic device by applying with CRISPR diagnostic can be provided a rapid, accessible, accuracy, and low-cost point-of-care (POC) medical diagnostics.

The scope of the study of this project is limited to, first, the fabrication technique of the paper-based microfluidic device focus only printing technique, second, using the red, blue, and yellow dye color solutions instead of the real amplification reagents, which are forward primer, reverse primer, RevertAid Reverse Transcriptase, and dehydration buffer, and the real samples, which are EnGen Lba Cas12a (Cpf1), fluorescent reporter/quencher probe, NEBuffer, crRNA, 6-FAM, and DEPC-treated water [2].

1.5 Report Outline

The rest of this report is organized as follows:

Chapter 2 Reviews the principles of Coronavirus or SAR-CoV-2, Current COVID-19 testing method, CRISPR-Cas12a-based assay, paper-based microfluidic device, and the mixing limitation of lateral flow.

Chapter 3 Illustrates all related equipment, materials, and prototypes design, clarify the solution preparation, and the methodology of paper-based microfluidic device fabrication and device testing.

Chapter 4 Demonstrate the result of the most effective condition to fabricate a paper-based microfluidic device which can be applied CRISPR-Cas12a-based assay with the most optimal condition and design. This will be achieved by a discussion based on the results.

Chapter 5 Conclude the project with the processes, results, and future works.

CHAPTER 2
REVIEW OF THEORY RELATED

2.1 Introduction

This chapter provides and review of theories from published articles related to this project. The related theories within this chapter consist of 4 main sections: A review of COVID-19 (section 2.2), which provided about an overview timeline of COVID-19, virology of COVID-19, and the life cycle of SAR-CoV-2. A review of current and advanced methods for testing COVID-19 (section 2.3), which mentioned about the standard method for detecting COVID-19 such as RT-PCR, RT-qPCR, and ATK method, and an advanced method like CRISPR-based assay for COVID-19. A review of paper-based microfluidic device (section 2.4), which provided about the history of both traditional microfluidics and paper-based microfluidics, the fabrication methods, and related equations for paper-based microfluidic device. A review of colorimetric assay (section 2.5), which mentioned about the advantages and disadvantages for each assay for determine the best assay to use in this project.

2.2 COVID-19

Since December 2019, a group of pneumonia patients with an unidentified cause, but who had similar symptoms with SARS and MERS, were first reported in Wuhan, China. On 8th December 2019, the first identified group of patients were epidemiologically associated with seafood market in Wuhan, which not only sold the seafood but also live animal, such as fowl and wild animals. The symptoms that had shown among this group of patients were high fever, cough, sore throat, headache, and difficulty breathe, and in the severe cases, they showed the symptoms of dyspnea and lung infection. On 31st December, the World Health Organization (WHO) received a notification from China about an unidentified disease for the purposes of monitor on this circumstance and preparing for the prevention of the disease's spread. Subsequently, Chinese researchers have discovered the cause of this newly developing illness was beta coronavirus, which is a species that has never been discovered before. The almost complete genome sequences of this novel coronavirus were first published

via the database of GISAID on 9th January 2020. The novel coronavirus was named 'SAR-CoV-2' by the international Committee on Taxonomic of Viruses on 11th February, and the disease 'COVID-19' named by the WHO [5].

2.2.1 Virology of SAR-CoV-2

The SAR-Cov-2 belong to Species: *Severe acute respiratory syndrome-related coronavirus*, subgenus: *Sarbecovirus*, Genus: *Betacoronavirus*, and in Family: *Coronaviridae*. It has a spherical shape with diameter around 80 – 160 mm. The RNA genome has the length around 26 Kb – 32 Kb, which makes it is the longest strain of known viruses. The main structures of SAR-CoV-2 consist of Spike protein (S), Membrane protein (M), Envelope protein (E), which are covered on the virus surface, and Nucleocapsid protein (N), which is located inside of the envelop [6,7].

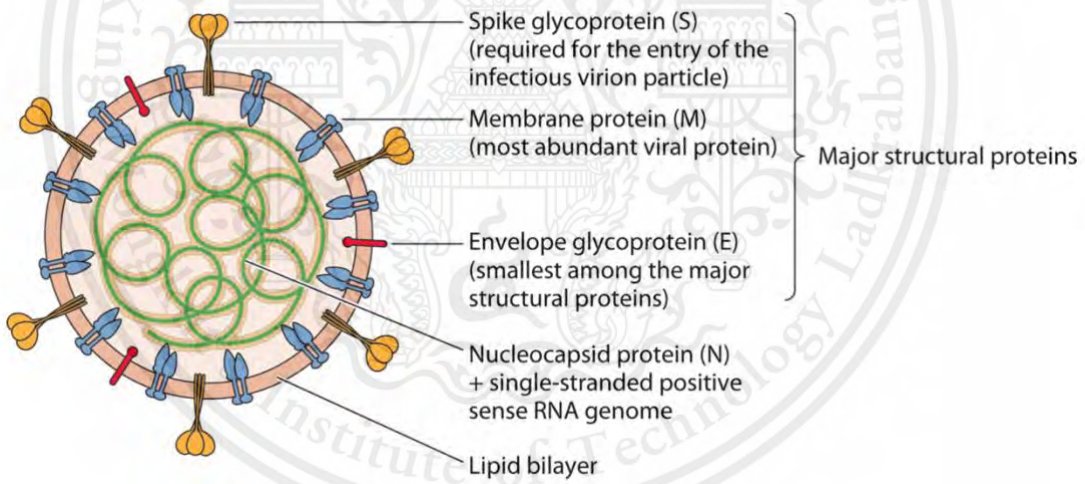

Figure 2-1. Structure of SAR-CoV-2 virus [8]

The functions of SAR-CoV-2's main proteins are:

S protein is the protein that has a power to attach the virus particle to the host cell receptor, normally is an Angiotensin Converting Enzyme 2 (ACE2) receptor, to help the SAR-CoV-2 virus fusion and enter into the host cell. S protein is divided into 2 subunits, which is S1 and S2. The S1 facilitates the virus's adherence to the host cell, and the S2 aids in its fusion with the membrane of the host cell [7].

M protein is the most commonly found of the protein in the virus particles, which provides a specific shape of virus envelope. The interaction between S protein and M protein causing the facilitating into new virions. The binding between M protein and N protein causing the stabilization of the virions' internal core to complete in virus assembly. The interaction between M protein and E protein helps in virus envelope production. The interaction between M protein and M protein helps to maintain the virus structure [8].

E protein is the smallest protein which has a multifunction in the role of disease pathogenesis, virus assembly, and virus release. It is an important protein to produce a virus and virus maturation. So, absence of E protein will make the virus disfunction [8].

N protein has the function with the genome of the virus, which bind with M protein to complete the virus assembly [8].

2.2.2 The life cycle of SAR-CoV-2

SAR-CoV-2 particles attach to the host cell for binding between S protein and host cell receptor, this specific binding cause the interaction between SAR-CoV-2 and host to fuse and release RNA inside the host cell. After that, the 2 Open Reading Frames (ORF1a and ORF1b) of the RNA are primary translated into pp1a and pp1ab. Both of polyproteins (pp1a and pp1b) is post translated into the individual non-structural protein (NSPs). The assembly between NSP12 and others form a replication and transcription complex on double-membrane vesicles (DMVs) to build a shield for viral genomic replication and transcription. Then, the viral RNA is translated into structural proteins of SAR-CoV-2 consist of Spike protein (S), Membrane protein (M), and Envelope protein (E), located in Endoplasmic Reticulum (ER). The structural proteins then transit to Golgi Body to assemble the virion, where the viral genome and N protein are synthesized in the cytoplasm and assemble into nucleocapsid. Finally, both structural proteins and nucleocapsid are integrated and form new virions, then released out of the infected cell by exocytosis [9,10].

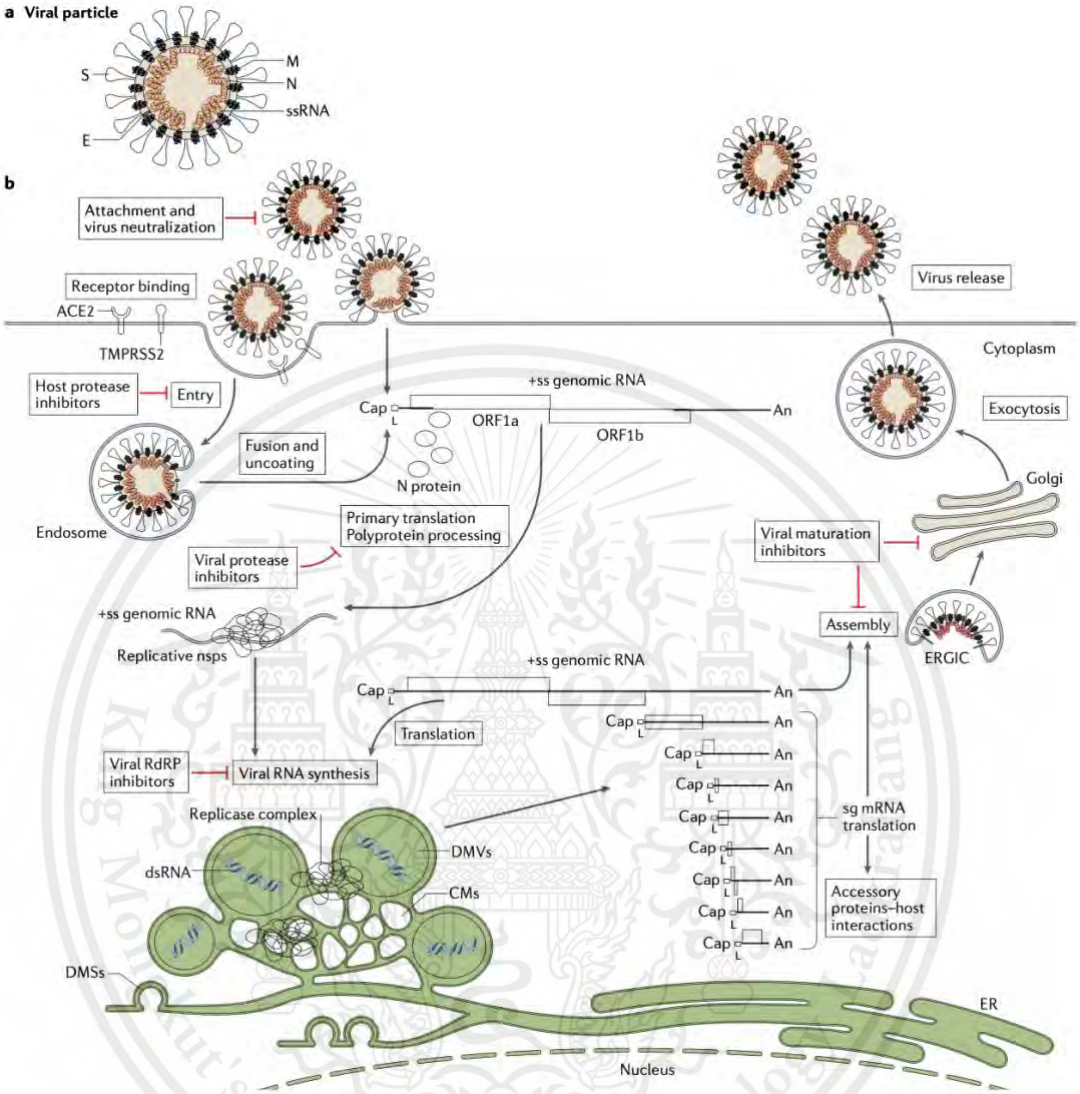

Figure 2-2. The life cycle of SAR-CoV-2 [9]

2.3 Current methods for testing COVID-19

2.3.1 Reverse Transcription Polymerase Chain Reaction (RT-PCR) test

A Reverse Transcription Polymerase Chain Reaction (RT-PCR) is the golden standard for COVID-19 detection. Originally, PCR is the general technique used for detecting nucleic acid of the viruses and amplifying the quantity of DNA copies, but if PCR is applied to detect the COVID-19, which is a virus that has only ribonucleic acid (RNA), so it requires to do the reverse transcribed to convert RNA to be the complementary DNA (cDNA). After the transcription and amplification, the result can be analyzed to detecting the COVID-19 virus. PCR technique provides a high sensitivity and specificity, up to 93 – 95%. However, this technique is time consuming and expensive because the cost of the apparatuses and only technicians that can be proceed the PCR test [11,12].

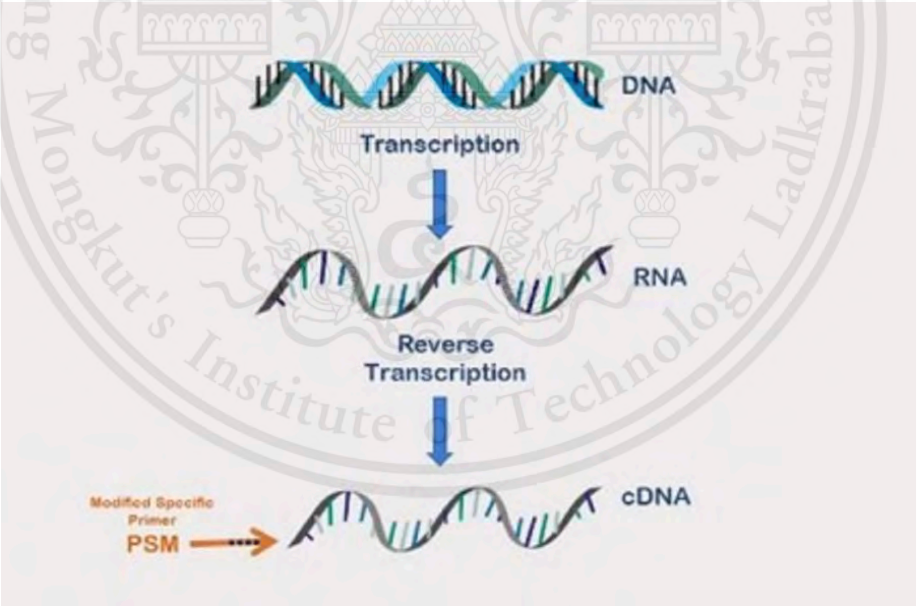

Figure 2-3. The illustration of the reverse transcribed to generate a cDNA [13]

2.3.2 Reverse Transcription Quantitative Polymerase Chain Reaction (RT-qPCR) test

To date, PCR technique was developed to be several techniques for improving the sensitivity and specificity. One of developed PCR techniques that can be able to amplify RNA of COVID-19 virus and measure the fluorescent signal is RT-qPCR. The difference between RT-PCR and RT-qPCR is RT-qPCR used the fluorescence quenching probe binds with DNA. To measure both DNA concentration and fluorescent signals, after virus RNA is reverse transcribed to be cDNA, the cDNA is binded with the fluorescence quenching probe. During the amplification step, the fluorescence quenching probe is cleaved to cut the reporter out of quencher to produce a fluorescent signal, and it can be measured by a photodetector [11,14].

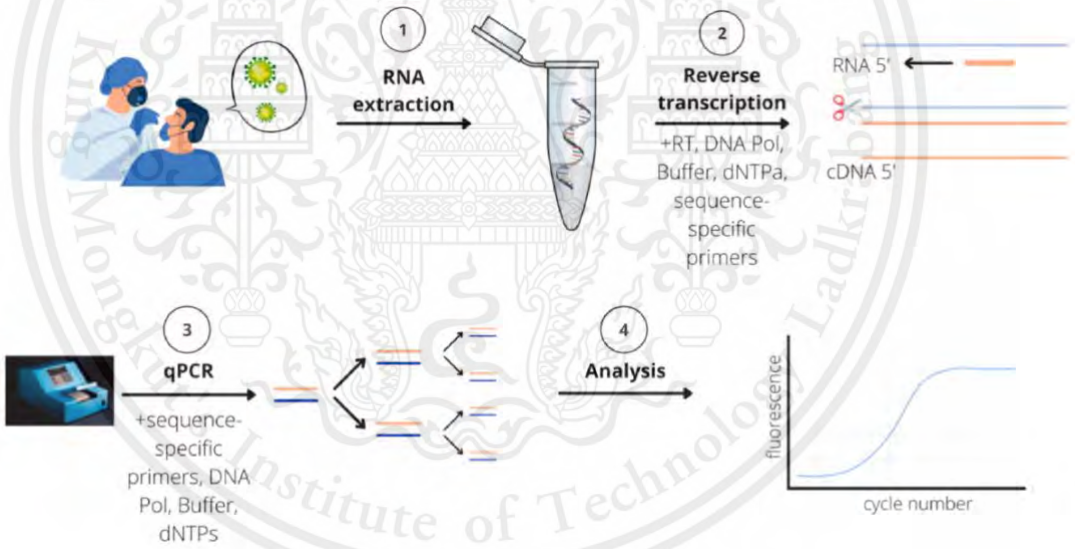

Figure 2-4. The illustration of qPCR processes [11]

2.3.3 Antigen Test by using Antigen Test Kit (ATK)

Antigen test is another COVID-19 detection method, which can be directly detect the antigens of SAR-CoV-2 and specified by the antibody. Antigen is some parts of virus that has ability to activate the immune system. In the case of COVID-19 detection, the antigen from SAR-CoV-2 virus is defined by using the spike proteins (S),

envelope protein (E), and Nucleocapsid protein (N). This technique is easy to access and cheap. The overall process of this technique is only 10 – 15 minutes, which the kits can portable to use at POC test and convenient to use. However, compared with the PCR technique, the antigen test by using ATK has the sensitivity only 49% [12,14].

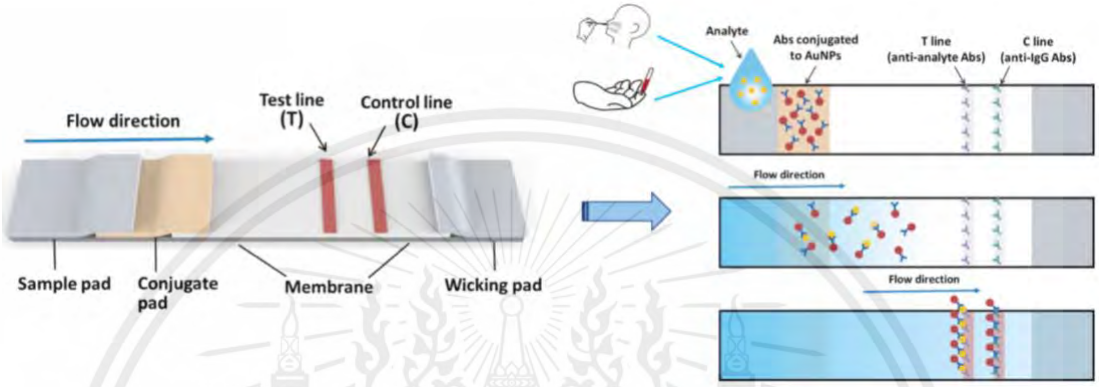

Figure 2-5. The illustration concept of dipstick assay and antigen test [15]

2.3.4 The advance technology for COVID-19 detection

2.3.4.1 Clustered Regularly Interspaced Short Palindromic Repeats (CRISPR)

In 1980s, Clustered Regularly Interspaced Short Palindromic Repeat or CRISPR was discovered and subsequently became a robust tool for genome editing in 2012 since their ability to edit genome was confirmed. The construct of CRISPR-Cas system consists of 2 main parts which are a CRISPR RNA sequences (crRNA), it is a guide RNA that act as an identifier and navigator for Cas endonuclease to the target sequences, and Cas endonuclease, which is the formation of protein complexes that contain crRNA and it can be an enzyme to cleaves the target sequences. Currently, due to the development of CRISPR-Cas system, the Cas protein is divided into 4 types based on their functions, as shown in Figure 2-6 that consist of: Cas9, Cas12, Cas13, and Cas14. This can be improving the field of using for CRISPR technology is not only just a robust tool for genome editing but also included in the field of infectious diseases diagnostic. So, the CRISPR-Cas system is divided into 2 classes based on their functions and Cas protein which are ClassI, is the CRISPR-Cas system that used to

adapt the immune system against with external elements, and ClassII, is the CRISPR-Cas system that used to edit the genome and diagnose the infectious diseases [16, 17, 18]

Cas effector	Cas9	Cas12	Cas13	Cas14
Illustrations	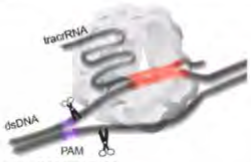	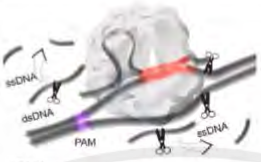	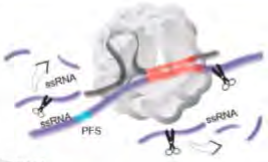	
Guide RNA	tracrRNA:crRNA	crRNA	crRNA	tracrRNA:crRNA
Nuclease domains	RuvC and HNH	RuvC	HEPN	RuvC
cis-cleavage	dsDNA	DsDNA or ssDNA	ssRNA	ssDNA
trans-cleavage	without	ssDNA	ssDNA	ssDNA
PAM/PFS required	NGG	(T)TTN	Non-G	without
Spacer length	18-24 nt	18-25 nt	22-30 nt	20-40 nt

Figure 2-6. The illustration of the CRISPR-Cas type [17]

2.3.4.2 CRISPR-Cas12a System for COVID-19 Diagnostic

During the COVID-19 pandemic, many diagnostic methods have been developed with the desired functions such as high sensitivity, high specificity, easy to access, low-cost, rapid, etc. CRISPR is the one of technology that developed and approved by the World Health Organization's (WHO) for using as COVID-19 detector.

The CRISPR-Cas12a is the diagnostic CRISPR-Cas system, that consist of a guide RNA (crRNA) and Cas12a, which applied in a new developed system called DNA Endonuclease-Targeted CRISPR Trans Reporter (DETECTR) to detect the sample RNA of SAR-CoV-2 from either nasopharyngeal or oropharyngeal swab. This system combines with amplification reagent for amplification to increase target sample and the crRNA navigate the Cas12a to the target sequences of the sample. The target sequences are cleaved by Cas12a, and the reporter-quencher is cleaved the reporter out of quencher to let the fluorescent signals illuminated. To amplify and detect the target samples, it requires to proceed the reaction by controlling the temperature at 39 °C for 30 and 15 minutes, respectively. This new technique is not only showing the result as a qualitative detection, but also showing in quantitative detection. The result of this system has high sensitivity and specificity, rapid, and low-cost, which can be compared with any conventional diagnostics [16, 19].

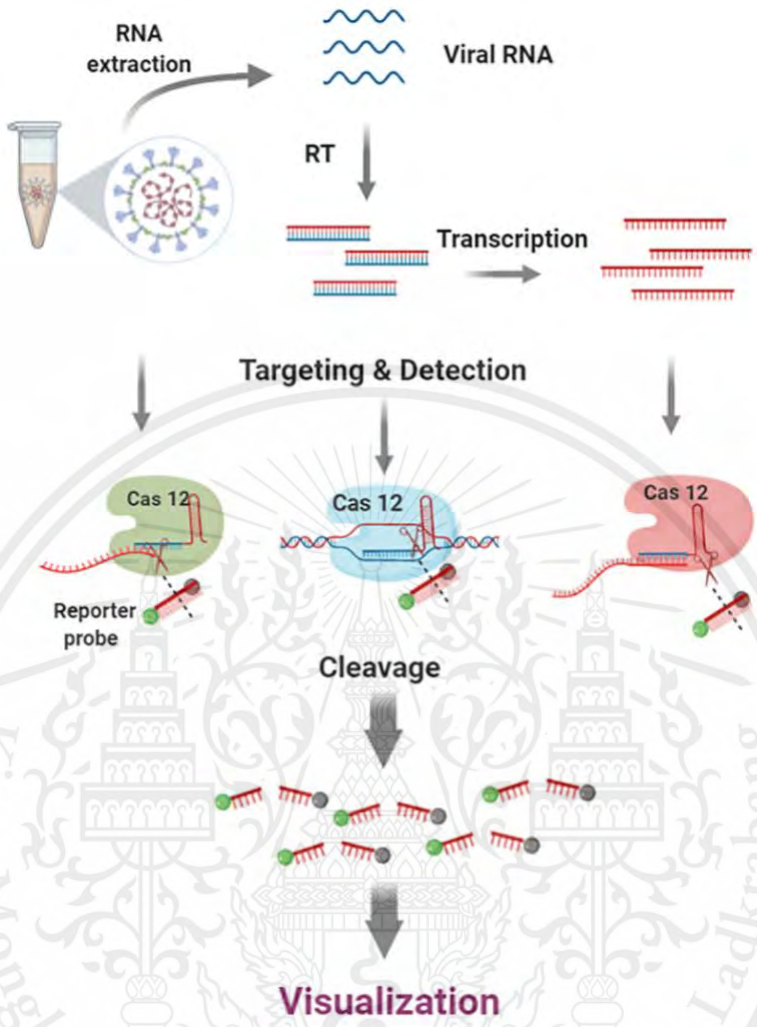

Figure 2-7. The illustration of SAR-CoV-2 detection by using CRISPR-Cas12 based systems [16]

2.4 Microfluidic Device

2.4.1 Traditional Microfluidic Device

A microfluidic device is a very tiny size device that fabricated by microfluidic technology, which it is a technology that has precisely control the scale of equipment to around 10 – 100 μm. When microfluidic technology was introduced in the early 1990s, it has evolved the field of analytical measurement at the Point-Of-Care (POC) application. At that time, many groups tried to develop microfluidic devices to achieve the purposes of laboratory outside setting, by removing the extensive external pumps,

valves, and other instruments that decreased their portability, to apply their applications onto microfluidics and proceed by using capillary flow instead. To date, microfluidic devices have been developing and used as a platform to be an analytical device in many fields of medical and chemical application, such as Lab-On-a-Chip (LOC). The main advantages of this technology are precisely control the volume of solution, which reduced in the term of solution cost, and it can integrate many laboratories to proceed within one microchip. However, although a microfluidic device can be used to reduce solution cost, the fabrication cost of traditional microfluidic device is still very high. This is because the traditional microfluidic devices using glass, polymer, silicon wafer, etc. as the material to fabricate a microfluidic device, which are the highly expensive material. Moreover, the fabrication processes are very complicated, and the materials have poor flexibility, so the cost of the manufacturing is also increased. Especially, by using silicon wafer as a material of microfluidic devices, it requires a very large scale of production to produce and fabricate a very tiny microfluidic device. So, these disadvantages make a microfluidic device difficult to access in scientist and researcher. Therefore, Martinez et al. combined the concept of microfluidics and sough for a new material to replace the disadvantages of traditional microfluidic devices, which is a paper, to become paper-based microfluidic device [20, 21, 22].

2.4.2 Paper-based Microfluidic Device

After Martines et al. discovered a new material to combine with microfluidic technology and becomes paper-based microfluidic device, it has gradually attracted the interest of researchers due to its advantages that overcome a traditional microfluidic device and paper is a prevalent material that has very low cost to easily access, another excellent property of paper is, it has high biocompatibility with many reagents that can be combined in various chemical, biological, and medical applications. The paper-based microfluidic device transports the liquid by using capillary force without using the external pumps, or valves. So, it is a very convenience technique that has low-cost of manufacturing, provide an ease of accessibility, simplest fabrication processes, tiny solution usage, fast response, and user-friendly. Therefore, this is led paper-based microfluidic device to grow rapidly in the field of POC diagnostic because this

technology fulfills the WHO guidelines for an ideal POC diagnostic system, which is the ASSURED (Affordable, Sensitivity, Specific, User-friendly, Rapid & Robust, Equipment Free, and Deliverable). However, this technique still has big issues that required to consider, which are the devices' stability and the operation the complexity of assays in the device can be limited because the simplicity of paper-based microfluidic device makes it difficult to apply the complex or complicated assays. Nevertheless, the paper-based microfluidic device has been continue developing to overcome the issues and achieve to use it as an analytical device for every assay as it is possible [21, 23].

2.4.2.1 Historical of Paper-based Microfluidic Device

Paper was first identified in the world around 105 A.D. in ancient China. In the early 19th centuries, a litmus paper was developed by Gay-Lussac. In the period of 1850s to 1950s, paper-based sensors attracted the interested of many researchers which they have developed it for applying in various applications. In 1940s, Muller, Clegg, and his research group were the first team to develop the first prototype of paper-based microfluidic device using paraffin patterned on the filter paper by inserting a heat die onto filter paper, the paraffin was transferred to form hydrophobic barrier and hydrophilic channel on the filter paper. However, with the Nobel Prizes being awarded to Martin and Synge for their invention of paper chromatography, paper-based sensors became well known in 1952. The commercialization of paper-based sensors began in the middle of the 1960s, consist of the first dipstick assay for blood glucose detection, pregnancy test kit, which showed that the paper-based sensors got more attention to interested in developing paper-based sensing. In 1990s to 2000s, Paper-based tools for analyte detection have been developed gradually such as diabetes, cholesterol, diagnostic of infectious disease, etc. In 2007, the early paper-based microfluidic technologies are widely acknowledged to have been initiated by Whitesides' group of Harvard University. They applied a photolithography to precisely create a hydrophobic barrier on the filter paper by using a photoresist for the purpose of creation μPAD for quantitative analysis. However, applying photolithography to create hydrophobic barrier on the filter paper is the complicated fabrication method, and the cost that

require to use in this is expensive. So, this technique is not suitable for mass production and resource-limited setting [20, 22, 23, 24].

Since then, a variety of fabrication techniques have been presented as photolithography substitutes.

2.4.2.2 Fabrication Techniques of Paper-based Microfluidic Device

New opportunities to integrate and minimize the several types of laboratories for diagnostic and analytical purposes have been developing over past decades into a small paper-based microfluidic device, which can be applied in many fields. These developments have made new opportunities for lightweight, accessible point-of-care diagnostics feasible. However, although the first paper-based microfluidic technology had been developed by Whitesides' group since 2007, to fabricate paper-based microfluidic device for commercialize still lacking due to the ability to scale-up of the fabrication process to commercialize are not simple, easy, and low-cost. On the other hand, the alternative fabrication techniques were observed a new opportunity to reduce the complexity and cost of fabrication. Recently, in general, the paper-based microfluidic device can be fabricated by either patterning on the filter paper or cutting the filter paper to create the hydrophilic channel.

Fabrication processes of paper-based microfluidic devices consist of 2 main processes which are: designing the device for required application, patterning the design on filter paper, and applying the reagent for test in the devices. Here is the example of fabrication techniques, which are Wax Printing, Laser Printing, and Thermal Transfer Printing [25].

2.4.2.2.1 Wax Printing Technique

Wax printing is one of the most popular techniques for patterning paper due to its simplicity, convenience, and rapid technique, which uses only 15 minutes of fabrication processes. Wax Printing uses solid ink printers to pattern the hydrophobic barrier by applying the molten wax components onto the surface of filter paper, which is melted from solid ink printer. Then, the filter paper is heated to melt the wax and let

it penetrate through the thickness of filter paper. The resolution of wax printing technique is better than Thermal Transfer Printing technique, but it does not high like Laser Printing technique. However, most of applications did not require a very high resolution, so the resolution of wax printing is sufficient. Although the wax printing is very popular technique which has the most convenience to fabricate and rapid when compared with Thermal Transfer Printing and Laser Printing, but solid ink printers were discontinued and no longer being manufacturer since 2016. So, this technique will decline in the next soon future [26].

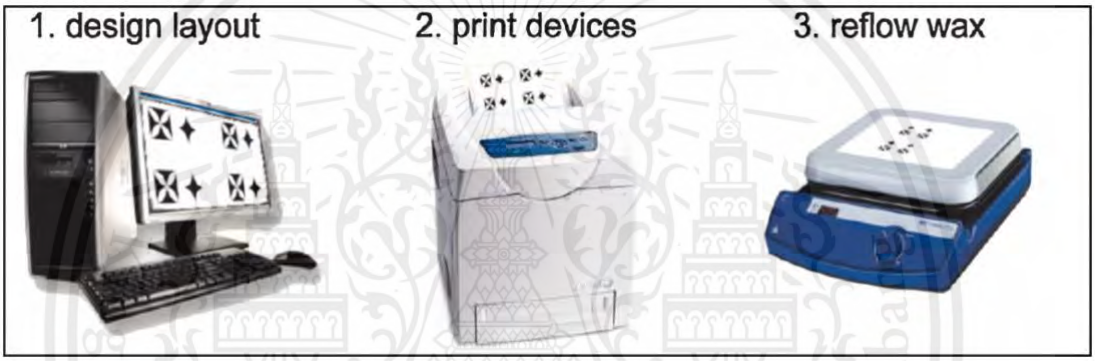

Figure 2-8. The illustration of paper patterning by using wax printing technique [26]

2.4.2.2.2 Laser Printing Technique

Due to discontinue in commercialize of solid wax printers in 2016, Day et al. were the first group that applied a new alternative fabrication technique of Laser printing, but unfortunately, their publication mistook to define the printer to be an inkjet printer.

In 2018, Ghosh et al. successfully to apply the commercial laser printer, which is HP Laser printer, for printing and patterning the paper by deposited the hydrophobic toner ink onto the filter paper. Then, the filter paper is heated to melt the toner and it let penetrate through the thickness of filter paper. To compare between wax printing, laser printing and Thermal Transfer Printing, a laser printing require the higher temperature and longer heating time to heat and melt the toner. The laser printer has higher resolution than both wax printing and thermal transfer printing, which printed at

600 dpi, so it can be ensure for homogeneity and repeatability of fabrication. Unfortunately, the laser printers, that were used by Day et al. and Gosh et al., were discontinued. However, this technique is the beginning choice for many researchers due to it is easily to access and the cost of laser printer cheaper than a solid ink printer [25, 26, 27].

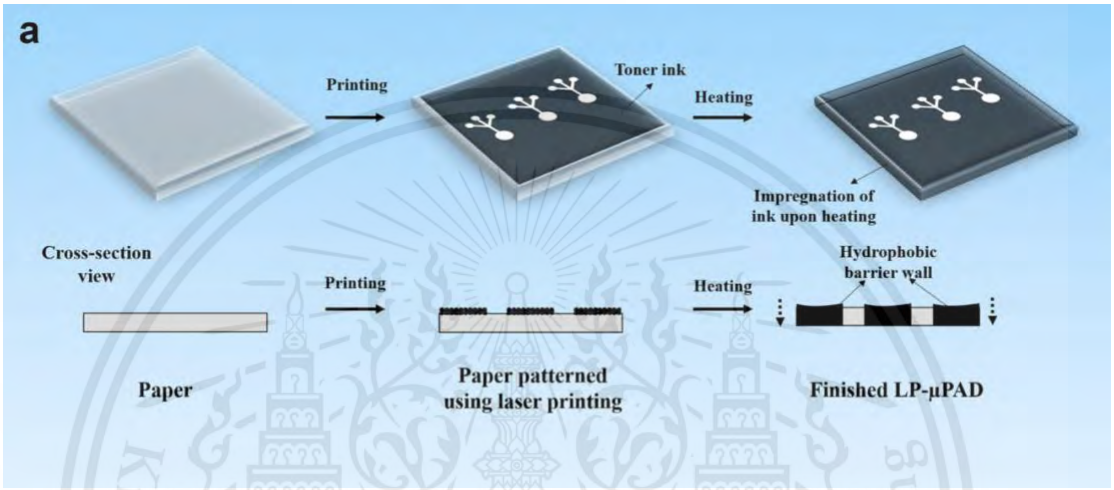

Figure 2-9. The illustration of paper patterning by using laser printing technique [25]

2.4.2.2.3 Thermal Transfer Printing Technique

Thermal Transfer Printing is a new technique to apply the thermal transfer printer for printing and patterning the hydrophobic barrier onto the filter paper. In 2022, Ruiz et al. are the first group that used HRPT Thermal Transfer Printer to fabricate paper-based microfluidic device. The thermal transfer printers use heat to apply a wax-based solid ink from a carbon ribbon onto the filter paper. Typically, thermal transfer printers are used to print the barcodes and labels and they usually used to print only A4 size. The limitation of thermal transfer printers is, it able to print only on small surface area or on some specific materials. However, the thermal transfer printers achieved to fabricate a paper-based microfluidic device and the main advantage of this technique is the solid ink require lower temperature and time for heating and melting the solid ink than the laser printer. Nevertheless, the resolution of the thermal transfer printers are lowest when compared with Wax printing and Laser printing, although the resolution

of thermal transfer printing has low, the resolution of paper-based microfluidic device that fabricated by thermal transfer printer is enough to use as an analytical device [27].

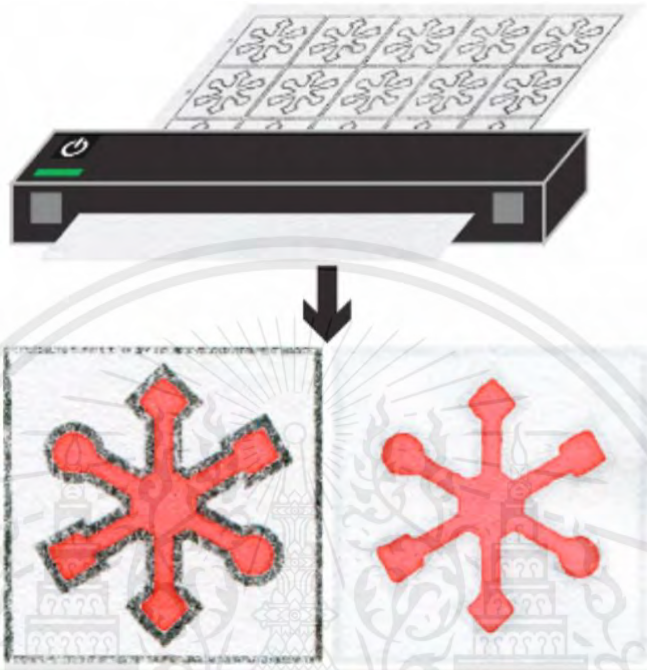

Figure 2-10. The illustration of paper patterning by using thermal transfer printing technique [27]

2.4.3 Lucas Washburn Equation

An equation that is used to describe the solution wicking through cellulose metrics materials, it was developed by Lucas and Washburn which is called 'Lucas-Washburn equation'. Cellulose metrics in some materials, such as paper, is defined the structure as the groups of cylindrical tubes where can be transport the solution by using capillary action in one dimension. This equation took as an equilibrium system which viscous force, capillary force, and hydrostatic force are equal. The conditions that Lucas and Washburn were designed to consider for this equation are evaporation doesn't take place, the inertial and gravitational force are negligible, uniform porosity in the material, hydrophobic barrier does not account to be an effect of solution wicking, solution wicking by laminar flow which has low viscosity, and the quantity of adding

solution does not be considered. From those conditions, Lucas and Washburn could generate the equation as:

$$L(t) = \sqrt{\frac{rt\gamma cos\theta}{2\mu}} \quad (1)$$

Where

L = distance travelled

r = average pore radius

γ = surface tension of the flowing liquid

θ = the contact angle between the capillary wall and the liquid

μ = the dynamic viscosity of the liquid

t = time

However, based on the consideration from Lucas and Washburn, there still has misconduct of some conditions that can be effect with the result of experimental. In real characteristics of paper's cellulose is, it does not the uniform porosity throughout the material, but it connected together like a network model [21, 28, 29].

2.4.4 Lucas Washburn Equation with resistance from hydrophobic barrier (Modified Washburn Equation)

In some applications of paper-based microfluidic devices that have multiple steps analysis, they must control the solution speed, which is called 'imbibition speed', to perform a testing with required time. However, this condition cannot be applied with the Lucas-Washburn equation because this equation does not account the controllability of solution speed but declare in the term of decreasing speed with respect to time. Therefore, several developments of defining equation have been accomplished to account for controlling the imbibition speed in paper-based microfluidic devices.

Li et al., Böhm et al., and Evans et al. reported that the hydrophilic channel width has an effect on imbibition speed when it flows through the channels with hydrophobic barriers. Li et al., Böhm et al., and Evans et al. made an assumption that the Lucas-Washburn equation was not consistent with their observations, this is because the Lucas-Washburn equation is predicted to independent of the channel width. This observation showed that a narrow hydrophilic channel is induced the imbibition speed to be reduced. The explanation of this observation was described by Li et al., which the viscous force exerted by hydrophobic barrier that can cause the imbibition speed to be dependent of the channel width.

Hong et al. [28] demonstrated the research related to the dependence of imbibition speed of the channel width. The results showed that, the imbibition speed is reduced by the surface tension at the hydrophobic barriers, which acts in the opposite direction of the solution flow. From their observations, paper was considered to be a network of capillary tubes which aligned in parallel direction inside the paper and in each capillary tube, it has a contact angle between capillary tube-to-capillary tube (θ) or capillary tube-to-hydrophobic barrier (θ_b) which θ_b will be more than θ to inhibit the imbibition pass barrier, as it can be shown the flow characterization in this illustration and equation:

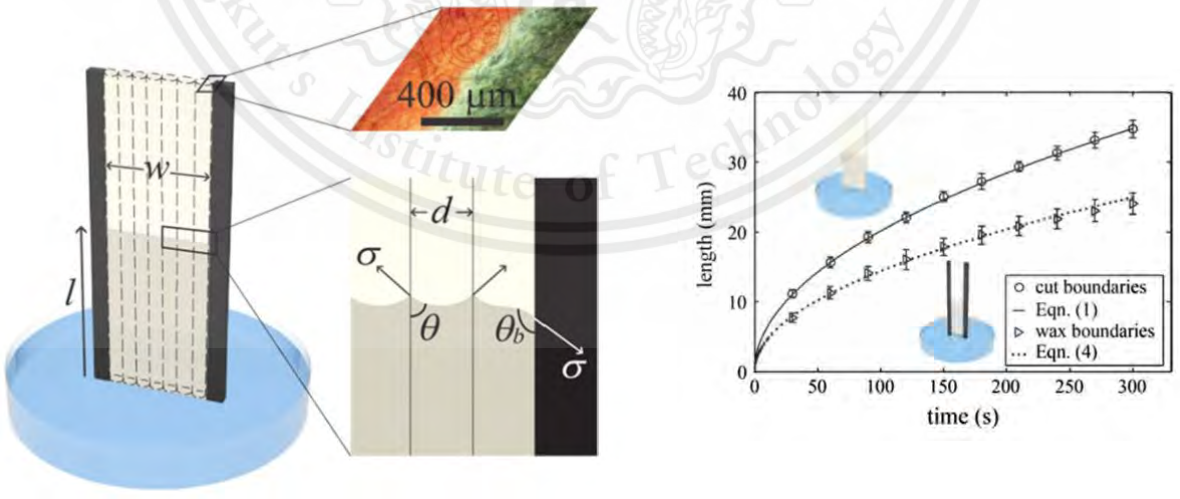

Figure 2-11. The illustration of comparison between imbibition in paper channel with hydrophobic barrier and without hydrophobic barrier. The paper channel is assumed to provide many capillary tubes aligned throughout the paper. The contact angle

between capillary (θ) less than 90° while the contact angle between capillary tube-to-hydrophobic barrier (θ_b) less than 90°. So, the the imbibition speed is reduced by the surface tension at the hydrophobic barriers [28]

$$l_m(t) = \alpha l(t) = \sqrt{\left(1 + \beta \frac{d}{\phi^{\frac{1}{3}} w} \frac{cos\theta_b}{cos\theta}\right) \frac{\sigma}{\mu} t} \quad (2)$$

Where

Lm = imbibition length

k = proportional constant

β = the length of contact line with the wax boundaries

d = pore diameter

ϕ = porosity of the paper

w = channel width

θ_b= contact angle of a capillary adjacent to a wax boundary

θ = contact angle in a capillary

σ = the surface tensions

μ = the dynamic viscosity of the liquid

t = time

2.4.5 Limitations of Mixing on Paper-based Microfluidic Device

The one of factors that are dependent to the accuracy and efficiency of biomedical and biochemical reaction is the mixing between analyte and sample. Thus, the effective mixing is very important for the detection step before the result is analyzed [30].

In the simplest flow for mixing of paper-based microfluidic device, that can be achieved for the development of diagnostic and currently available in commercial market, is the Lateral Flow Assays of a pregnancy test strip. The standard of sample flow through the paper-based microfluidic device for an immunoassay is Lateral Flow

Assays (LFAs) by utilizing capillary force to drive the sample to the detection zone, which the sample penetrated through the device and analytes are bound to detection analytes in control line and test line that where specific antibodies are located in, for generating visible signals as line banding [22].

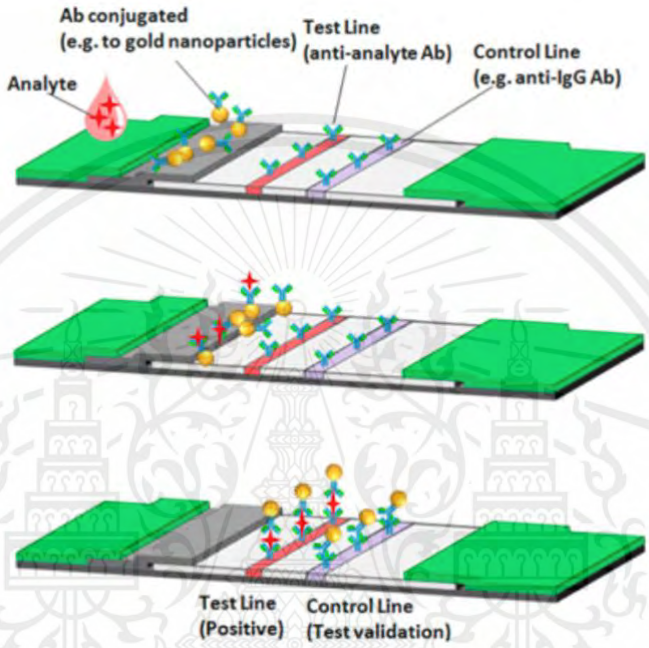

Figure 2-12. The illustration of lateral flow assay [22]

Although the lateral flow assay is the technique that simple and easy, the lateral flow assay can be only used for qualitative detection. Currently, the one of purposes to develop the paper-based microfluidic device is the integration of multiple steps in each assay into one device to reduce the cost of production, easy to use, and increase the reliable function, which can be resulted in both qualitative and quantitative detection.

Unfortunately, only the capillary force and sample diffusion to drive the sample through the paper-based microfluidic device for achieving the mixing efficiency are not enough and cannot control all the steps throughout the assays because they have a low Reynolds number of sample flow. Additionally, the capillary flow through paper-based microfluidic device is nonuniform, less efficiency, less predictable, and less controllability than the traditional microfluidic devices due to the issues of asymmetry of porosity and dimension of the paper structure, which effect with the controllability

and uniformity of effective mixing [31]. In order to enhance the mixing efficiency of the paper-based microfluidic device, the mechanisms of mixing can be broadly categorized into two types: laminar advection and chaotic advection. The laminar advection using an overlapping of the channel to increase the interface area between different sample to enhance the mixing efficiency, while the chaotic advection using a complicated geometric channel structure to increase the interface contact surface area of two samples or employing the external source for exsert the force to enhance the sample mixing. the several enhance mixing efficiency methods are broadly categorized into 2 types which are active micromixers and passive micromixers.

The external forces, such as piezoelectric, surface electric field, etc., are employed to generate the chaotic advection in the active micromixer' system, which makes the sample mix easily and effective, but however, the disadvantages of active micromixer are the addition external source is required, the increasing of production cost, and it is not easy to use [32].

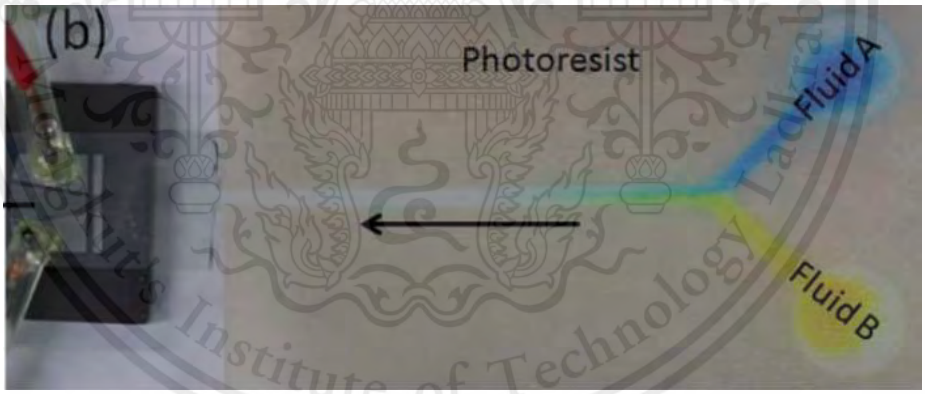

Figure 2-13. The illustration of active micromixer set up which uses a SAW as an external force to enhance the mixing efficiency [31]

Rather than using external forces, the passive micromixers enhance the mixing efficiency by improving the interface of the sample, or changing the geometric of device channel, such as serpentine shape or herringbone structure. Either chaotic advection or laminar advection of sample passive through the complex geometric can be enhanced the mixing efficiency. The advantage of passive micromixer system is the

external sources are not required. However, the complicated geometric of device channel is difficult to design and fabricate on the filter paper [33].

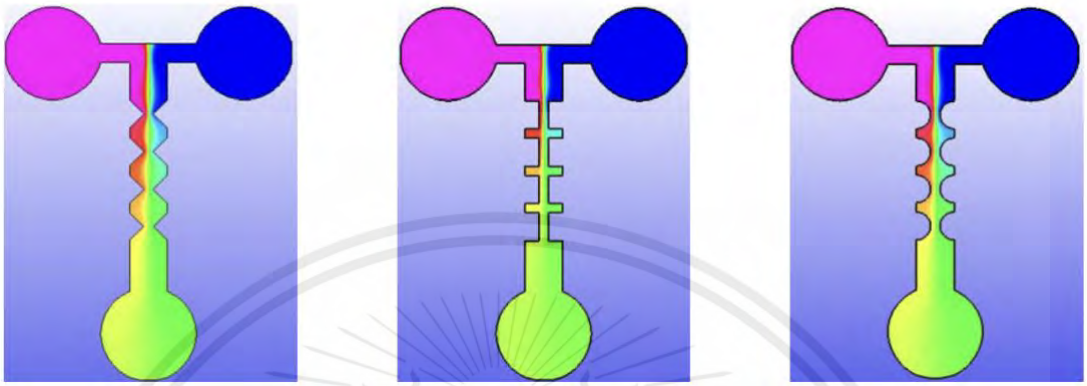

Figure 2-14. The illustration of passive micromixer which uses the complex geometric of mixing channel to enhance the mixing efficiency [32]

To date, it has few publications about using he paper-based microfluidic device as a sample mixer and concerning about the mixing limitation on the devices. The examples of publication showed the method that they used in both active and passive micromixer, which are Ilhoon et al. [05] developed a microfluidic rapid mixer by applying a passive mixer as an overlapping of the channel, and Rezk et al. [31] developed a paper-based active mixer by inducing 30 MHz the surface acoustic waves to the channel.

2.5 Colorimetric Analysis

In order to analyze the effective of sample mixing in microchannel, the grayscale analyzing is the common technique that measured by measuring the standard deviation of the color reference or the average of pixel intensity. Nevertheless, this technique requires the intensity of contrast between 2 samples, which one sample should be bright color or colorless, while the another should be dark color to get the good result of grayscale analyzing. This is the limitation of the grayscale analyzing technique because type of samples that can be used for the assays and used to analyze the mixing efficiency is limited.

Another method for analyzing the mixing efficiency is RGB technique, which is the only one technique of colorimetric. As similar with grayscale analyzing, the RGB technique is also limit to the access of sample selection because one of sample should be red, green, or blue color (primary color), while the another should be colorless [31].

The one of accurate color analyzing technique is Hue, which from the HSV color model. Hue is the color within the visible light spectrum appear as the mean value of any analyzed colors. The intensity and brightness of color do not affect with the value of color analyzing, which means the changing in different color is no difference in Hue value. This will be help for colorimetric analyzing and remove the previous limitations.

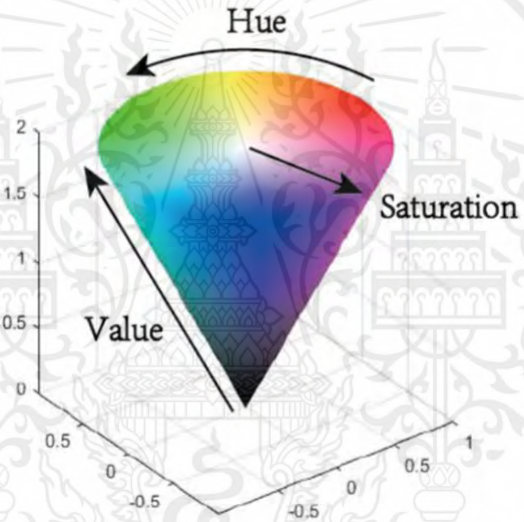

Figure 2-15. HSV color model [34]

2.6 Chapter Summary

Since December 2019, A Coronavirus Disease (COVID-19) was first reported in Wuhan China. It is an infectious disease, caused by the SARS-CoV-2 virus. The main structure of SAR-CoV-2 consists of Spike protein (S), Membrane protein (M), Envelope protein (E), which are covered on the virus surface, and Nucleocapsid protein (N), which is located inside of the envelop. The SARS-CoV-2 virus enter into the host cell by S protein to infect and replicate themselves to spread throughout the host body. To detect the COVID-19 disease, RT-PCR is the golden standard method for COVID-19 detection which provides a high sensitivity and specificity. RT-qPCR is developed

from the RT-PCR method, which can be detected in both qualitative and quantitative result. However, both methods need have high cost and time consuming, so ATK method is developed to reduce the time and increase convenience of use, but the sensitivity of this method is only 49%. So, CRISPR-Cas12a is developed to be a new COVID-19 detection method, which provides a high sensitivity and specificity like RT-PCR method, but easy to use and time saving like ATK method. In order to integrate all steps of CRISPR-Cas12a method, paper-based microfluidics is selected to use due to its ability that can be used as a POC diagnostic system, which provides a low cost, ease of use, simple, and time saving. The one of techniques that easiest to fabricate paper-based microfluidic device is printing technique, such as wax printing, laser printing, and thermal transfer printing. An equation that used to describe the solution wicking through cellulose metrics materials is Lucas Washburn equation. However, it does not account the controllability of solution speed. So, Hong et al. [28] developed a new equation that related to the dependence of imbibition speed of channel width, which called 'a modified Washburn equation'. Moreover, the one of limitation of paper-based microfluidic device is the mixing between analyte and sample. To increase the property of mixing, both active and passive micromixers were introduced. Lastly, to analyze the effective of sample mixing in microchannel, grayscale and RGB is the common technique for analyzing, but it has a limitation of the required sample types. The one of accurate color analyzing technique that was provided in this project is Hue from HSV color model.

CHAPTER 3
METHODOLOGY

3.1 Introduction

This chapter provides the related materials and equipment utilized throughout this project (section 3.2). The fabrication processes of paper-based microfluidic devices, including prototype designs, material selection, and techniques for patterning hydrophobic barriers, are detailed in this chapter (section 3.3). Furthermore, this chapter also describes about the experiment set up for device testing (section 3.4).

3.2 Related materials and equipment

- 2 – 20 μl micropipette (Precipette^{TM}, USA)
- 20 – 200 μl micropipette (Precipette^{TM}, USA)
- Red dye solution of food coloring (Best Odour Co., Ltd, Thailand)
- Green dye solution of food coloring (Best Odour Co., Ltd, Thailand)
- Blue dye solution of food coloring (Best Odour Co., Ltd, Thailand)
- Whatman 3MM Chr Chromatography Paper (Whatman^{TM}, USA)
- Whatman no.1 filter paper (Whatman^{TM}, USA)
- Double Rings No. 102 filter paper (Double Rings, Thailand)
- Hotplate (FOURE E'S, China)
- Hot air oven (Binder, Germany)
- Electric Oven (Magic Home Appliance, Thailand)
- HP Laser MFP 135a printer (HP, Thailand)
- HPRT MT800 portable A4 Thermal Transfer Printer (HPRT, Germany)
- Oven Thermometer (Shopee, Thailand)

3.3 Fabrication processes of paper-based microfluidic device

3.3.1 Device Design

During the project, all of device's designs were created in AutoCAD 2023 program to control the accuracy of device's dimensions for patterning hydrophobic barrier on the filter paper.

The 1st prototype design, the total length of device is 20 * 20 mm including with white background. It is the simplest design with one inlet and testing reservoir connected by one-way hydrophilic channel line. Both sample inlet and outlet reservoirs radius are 2 mm, width of the hydrophilic channel is 2.5 mm, and the length of hydrophilic channel is 10 mm. The design of first prototype is shown in Figure 3-1.

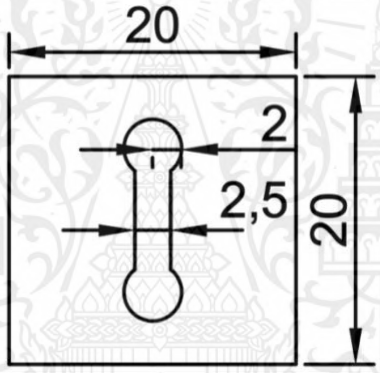

Figure 3-1. The design of the first prototype

The 2nd prototype design, all of parameters are the same with the first prototype but in this prototype, the background is added. The design of second prototype is shown in Figure 3-2.

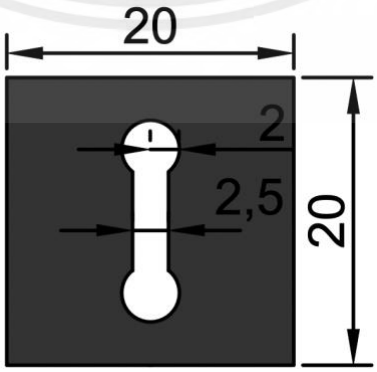

Figure 3-2. The design of the second prototype

The 3rd prototype design, all parameters still same with the first, and second prototype but in this design, line thickness around the hydrophilic channel is changed to be 0.5 mm. In order to provide a good hydrophobic barrier, 0.5 mm of line thickness will be applied in all design afterward. The design of third prototype is shown in Figure 3-3.

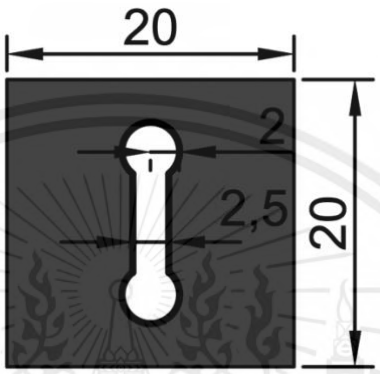

Figure 3-3. The design of the third prototype

The 4th prototype is designed based on a modified Washburn equation [28]. It is the set of 3 devices with different hydrophilic channel width and channel length. Both sample inlet and outlet reservoirs radius are 2 mm connected by hydrophilic channel which have channel width equal 1, 1.5, and 2 mm, respectively and hydrophilic channel length: 81.5, 66.5, and 57.6 mm. The dimensions of all designs are detailed in Figure 3-4.

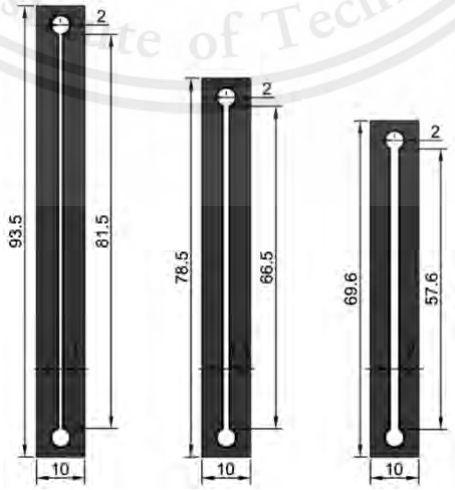

Figure 3-4. The design of the fourth prototype

The 5th prototype is also designed based on a modified Washburn equation [28]. Both sample inlet and outlet reservoirs radius are 4 mm connected by hydrophilic channel which channel width equal 4 mm and channel length equal 40.7 mm. The dimension of design is detailed in Figure 3-5.

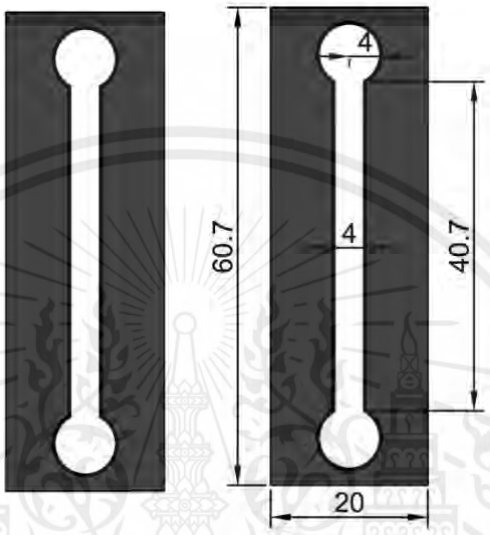

Figure 3-5. The design of the fifth prototype

The 6th prototype design is called 2 phases design. All sample inlet and outlet reservoirs radius are 4 mm. Both hydrophilic channels are 4 mm in width, which connected with each reservoir. The other dimensions of design is detailed in Figure 3-6.

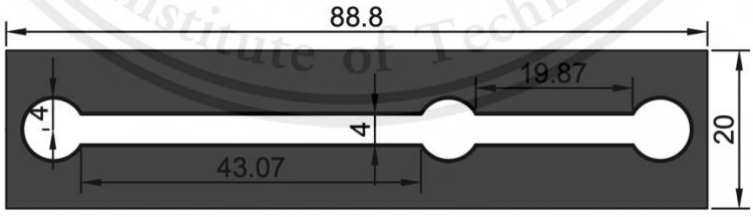

Figure 3-6. The design of the sixth prototype

The 7th prototype design is the set of 3 devices with different shapes used to compare the mixing efficiency consist of T-shape, Y-shape, and Cross-shape design from left to right side, respectively. Both sample inlet reservoirs have a radius of 2.5 mm, while outlet reservoir has a radius of 4 mm. The mixing zone of hydrophilic

channel has dimensions of 4.0 mm in width and 26.85 mm in length. In conclusion, the geometric dimensions of all designs are detailed in Figure 3-7

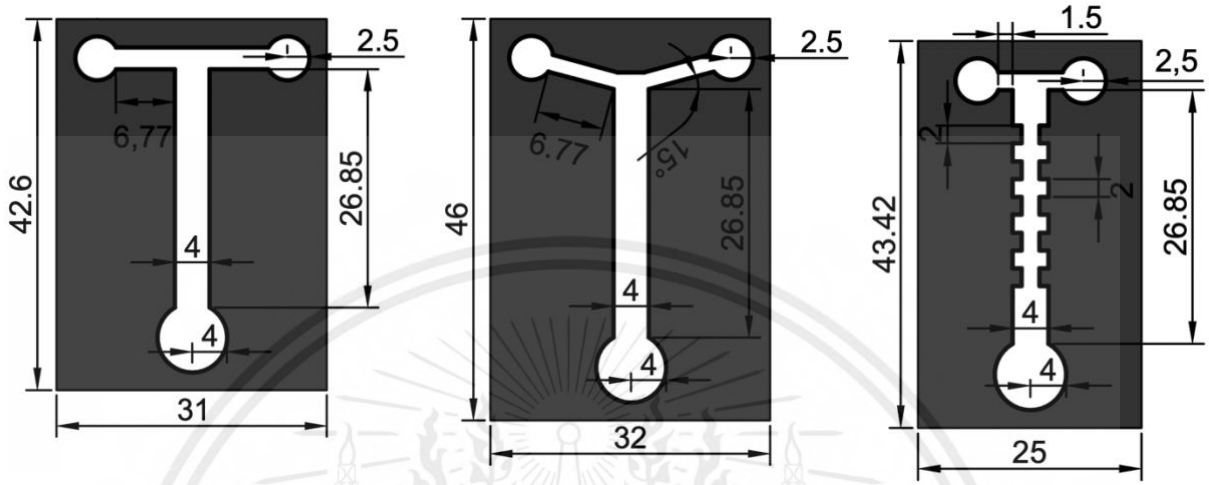

.

Figure 3-7. The design of the seventh prototype

The 8th prototype design, both sample inlet reservoirs were increased to be 4 mm of radius and the mixing zone of hydrophilic channel also was decreased to be 30 mm. In conclusion, the geometric dimensions of all designs are detailed in Figure 3-8.

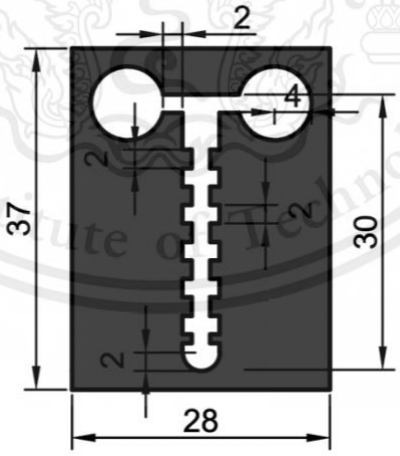

Figure 3-8. The design of the eighth prototype

3.3.2 Type of filter paper

To fabricate hydrophobic barriers on filter paper, it is important to choose the appropriate type of filter paper that allow samples to pass through. In this project, three types of filter paper which are Whatman 3MM chr, Whatman number 1, and Double ring 102 were tested. Each type of filter paper has a different pore size: 6 μm, 11 μm, and 8-10 μm, respectively.

3.3.3 Techniques for patterning hydrophobic barrier on the filter paper

The technique for patterning hydrophobic barrier on the filter paper that was used in this project is 'printing' technique. During the project, 2 printers were used to compare the results which are Laser printer and Thermal transfer printer.

Laser Printer, this technique relies on the toner ink which is printed on the surface of filter paper to pattern the prototype design and created hydrophobic barrier. The toner ink contained wax as a one of components to produce and create hydrophobic barrier on the filter paper. In this project, we used HP Laser MFP 135a printer to fabricate and patterning the filter paper.

HPRT MT800 portable A4 Thermal Transfer Printer, this technique relies on the carbon ribbon which uses heat to melt the carbon and then print the patterning hydrophobic barrier on the filter paper.

3.3.4 The number of printings for patterning on a filter paper

Increasing the number of printings for patterning the hydrophobic barrier resulted in a significant improvement in the resolution and hydrophobicity. In this project, after fabricated a hydrophobic barrier on the filter paper we tried to re-printing and re-patterning a hydrophobic barrier on the filter paper again for 1 time, 2 times, 3 times, and 4 times for HP Laser MFP 135a printer and 1 time, and 2 times for Thermal Transfer Printer to compare the result of water leakage.

3.3.5 Heating filter paper

During the project, three heaters which are hot plate, hot air oven, and electric oven were used to heat the devices for melting the printer's ink and soaked throughout the filter paper then the hydrophobic barrier of device was completely fabricated.

At the beginning of this project, the heating temperature and heating time were defined randomly for optimizing the best heating temperature and heating time to fabricate paper-based microfluidic devices. In term of testing with HP Laser MFP 135a printer, hotplate and hot air oven were used to heat the devices by randomly choose based on melting point of laser printer's toner ink. The six heating temperatures were selected to test in this project are 165, 180, 190, 200, 220, and 260 °C with the heating time of each temperature: 15, 30, 45 minutes, and 1 hour, respectively. For HPRT MT800 portable A4 Thermal Transfer Printer, an electric oven was used to heat the devices. The four heating temperature were selected to test are 90, 120, 150, 180 °C with heating time: 5 and 15 minutes, respectively.

After analyzed for optimizing the best heating temperature and heating time to fabricate paper-based microfluidic devices, the heating temperature at 120 °C with 15 minutes heating time is used to heat devices by using an electric oven.

Finally, the individual devices can then be taken out of filter paper sheet by cutting to make them ready for testing.

3.4 Device Testing

3.4.1 Testing the flow rate

In order to determine whether certain technique for patterning microfluidic channels has any influence on the result of fluid flow by considering heating temperature and heating time, the 3rd prototype design [Figure 3-3] was used to test by varying the heating temperature and the heating time followed by the details in heating temperature section (3.3.5). 5 µl of red dye solution was added into the sample inlet reservoir then the video and time were recorded while the red dye solution was flowing through the channel until it reached at outlet reservoir. To investigate the flow behavior

of each heating temperature compared with a Theoretical equation, which is Lucas Washburn equation, and Experimental equation, which is a modified Washburn equation, the video clip was converted into image sequences for 10 frames per second (fps), the images were selected from every 1 second until red dye color solution flowed to outlet reservoir. Then, the images were imported into ImageJ program to measure and analyze the distance of liquid flowing with respect to time by converting the measured pixels of image into known distance. Finally, plot the graph of experimental result, Lucas-Washburn equation, and Modified Washburn equation in MATLAB program.

3.4.2 Testing Characterization of Devices

In order to determine the minimum effective hydrophilic channel width that fabricated by HPRT MT800 portable A4 Thermal Transfer Printer, the 4th and 5th prototype design [Figure 3-4, 3-5] was used. After the devices were fabricated, red dye solution was added into sample inlet reservoir of each device in 10 μl increments until it leaks out of hydrophobic barrier, the time was recorded while the red dye solution flow through hydrophilic channel for 30 minutes. Then, measure the distance of liquid flowing in ImageJ program.

3.4.3 Testing Impact of Volume Quantity

In order to determine the effective volume quantity for the liquid flowing through hydrophilic channel within 30 minutes and 15 minutes based on the concept of target sample amplification and CRISPR detection steps, the 5th and 6th prototype design [Figure 3-5, 3-6] were fabricated. After fabrication, the devices were placed on both table surface and cooling rack to compare the result of flow behavior effected by contact surface. Then, the red dye solution was added into sample inlet reservoir by ranging volume from 30 μl – 70 μl in 10 μl increments and recorded the video and time for 15 and 30 minutes, respectively. To measure the flow rate and distance of fluid flowing, the video clips were converted into image sequences for 30 frames per second (fps) and selected the image results every one second until 15 and 30 minutes. Then,

this image results were measured the flow distance via ImageJ program and collected all data of distance to plot against with the experimental equation or a modified Washburn equation via MATLAB program to observe the most effective volume that related with the equation.

3.4.4 Testing Effective Mixing of Devices

3.4.4.1 Dye color solution preparation

The 10 ml of distilled water mixed with 150 µl of dye color. Blue and yellow dye were used to be as a sample (target sequences) and CRISPR reagent to mix and provide a green color at outlet reservoir for the detection step.

3.4.4.2 Mixing on Devices excluding Temperature Control

In order to determine the effective design for mixing between 2 sample by do not consider about the temperature control for incubating the reaction, the 7th prototype design [Figure 3-7] was selected to use. After fabrication, the devices were placed on cooling rack to suspend devices in the air that will not be inhibited by table surface. 20 µl of each blue and yellow dye color solution were added into each sample inlet reservoirs, waited until it mixed and flowed through mixing channel to outlet reservoir for 15 minutes. Then, photographs of each device were taken by iPhone X, which will be utilized for subsequent analyzing.

3.4.4.3 Mixing on Device with Temperature Control

In order to determine the effective design for mixing between 2 samples by considering about the temperature control for incubating the CRISPR reaction, the 7th prototype design [Figure 3-7] was selected to use. After fabrication, the devices were placed on cooling rack, which was placed on hotplate and control the temperature at 37 °C, to suspend devices in the air that will not be inhibited by table surface. 40 µl and 60 µl of each blue and yellow dye solution were added into each sample inlet reservoirs,

waited until it mixed and flowed through mixing channel to outlet reservoir for 15 minutes. Then, photographs of each device were taken by iPhone X, which will be utilized for subsequent analyzing.

After the cross-shape of 7th prototype design [Figure 3-7] was adjusted to be the 8th prototype design [Figure 3-8] by reducing the mixing channel length, the experiment was re-tested by using the volume of blue and yellow dye solution for 40 µl of each to observe the consistency of solution flow and also observe about the percentage of error from solution flow in length compared with the theoretical flow in length, which calculated from a modified Washburn equation [28].

3.4.4.4 Result Analysis

Once all of devices were completely tested and taken the photo by iPhone X, all photographs of result were analyzed in ImageJ program. To analyze the results via ImageJ program, the photographs of result were transformed the type of image from RGB to HSB Stack, then convert HSB Stack to Image. This conversion allowed to measure the Hue value by selecting the specific area of interest in the mixing area on the device's photograph and analyzed by using 'Plot Profile' to observe the Hue range for comparing between the reference Hue range of green color and the result of mixing between blue and yellow color on the devices.

3.5 Chapter Summary

This chapter encompasses the materials and equipment utilized throughout this project. During the project, the 8 prototype designs were used to conduct the experiment which patterned the hydrophobic barrier by printing technique using both laser printer and thermal transfer printer to observe the most proper fabrication method to produce paper-based microfluidic devices. After devices were fabricated, the 9 experiments conduct for testing the devices consist of testing the flow rate, testing the characterization of devices, testing impact of volume quantity, and testing the effective mixing of the devices. Moreover, all results were continue analyzed via ImageJ program.

CHAPTER 4
EXPERIMENTAL RESULT AND DISCUSSION

4.1 Introduction

This chapter provides a comprehensive experimental results and discussion, including all experiments that conducted during this project, along with the images and tables of result to illustrate on the outcomes for each test. In section 4.2.1, this provides a result of paper-based microfluidic devices that fabricated by a laser printer, including choosing the appropriate filter paper, enhancing hydrophobicity, and the influence of heater. In section 4.2.2, this provides a result of paper-based microfluidic devices that fabricated by a thermal transfer printer, including in device resolution and flow characterization according to the heating temperature and heating time. Lastly, in section 4.2.3, it provides results of device testing which are mentioned about the experiment set up in the previous chapter.

4.2 Result and Discussion

4.2.1 Result of Paper-based Microfluidic Devices Fabrication by Laser Printer

4.2.1.1 Choosing the Appropriate Filter Paper

In the pursuit of choosing the appropriate filter paper for this project, Whatman 3MM chr chromatography paper was firstly used. This paper was employed to create hydrophobic barrier of the first prototype by patterning it with laser printer and heating the devices by hotplate. After tested by adding 10 μl of distilled water into sample inlet reservoir, revealed that the distilled water completely leaked out of the barrier. This result was thought to be due to Whatman 3MM chr Chromatography paper has relatively high thickness and lower porosity, which affected with penetration of the laser printer's toner ink. So, the laser printer and hotplate were unable to form a hydrophobic barrier on this paper.

Next, the first prototype was modified by adding black background around the hydrophilic channel to become a second prototype, which enhancing the

hydrophobicity of the devices. In this experiment, Whatman no.1 and Double ring 102 filter paper were used. While both types of filter paper have similar property but small different with size of porosity, which Double ring 102 filter paper has lower porosity than Whatman no.1. They were fabricated and tested in same condition with Whatman 3MM chr Chromatography paper. From my observation, a complete hydrophobic barrier still could not be achieved on either type of filter paper. However, the results shown that the double ring 102 filter paper has better results than Whatman no.1 filter paper, which has more tendency to contain the distilled water inside of the hydrophilic channel, distilled water fewer leaks, and red dye solution tend to move along the hydrophilic channel better than Whatman no.1, as shown in Figure 4-1.

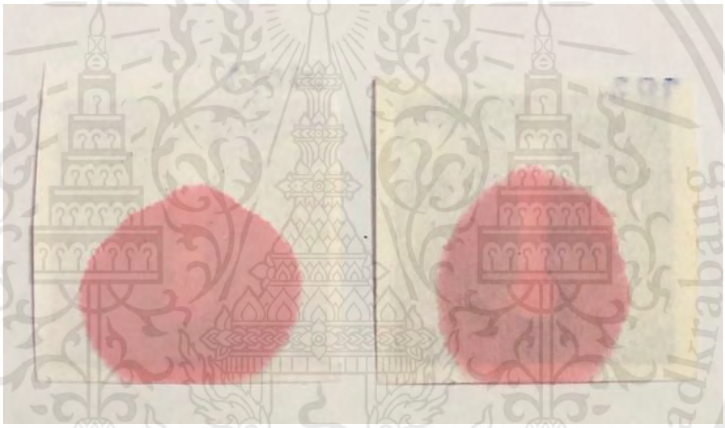

Figure 4-1. Comparing the flow tendency of red dye solution between Whatman no.1 and Double Rings 102 filter paper. (Left: Whatman no.1, Right: Double Rings 102)

Consequently, based on my observation, Double ring 102 filter paper was chosen to use in this project.

4.2.1.2 Enhancing Hydrophobicity by re-patterning the paper

After an appropriate filter paper was chosen from previous experiment, I also had another hypothesis that the increasing of background intensity was significantly improve hydrophilicity of barrier, which observed from the second prototype that was modified by adding black background around hydrophilic channel. So, from this hypothesis, the second prototype was modified by increasing line thickness around the hydrophilic channel to be 0.5 millimeters, as shown in 3rd prototype [Figure 3-3], and

also the devices were re-patterned for 1 – 4 times to accumulate the laser printer's toner ink onto the filter paper.

For the result, it was observed that 1-time and 2-time patterning could not be achieved to form hydrophobic barrier on the filter paper by observing from the dispersion of distilled water on the filter paper. However, 3-time patterning still could not be achieved but the dispersion of distilled water was reduced compared to 1-time and 2-time patterning, which means the tendency to contain the distilled water inside of the hydrophilic channel was improved due to increasing of hydrophobicity. The best result was achieved is 4-time patterning, it shown a significant improvement to contain the distilled water inside of the hydrophilic channel, with few leakages only at the sample inlet and outlet reservoir, as shown in [Figure 4-2].

Figure 4-2. Comparing the effect of resolution influence with the hydrophobicity of the hydrophobic barriers.

In conclusion, it can be observed that the increasing number of hydrophobic barriers is patterned, the increasing hydrophobic it becomes.

4.2.1.3 The influence of heater

Based on my observation from the 2 previous experiments, type of filter paper and number of re-patterning paper were not only the factors that affect with the penetration of laser printer's toner ink throughout the paper but also heater is another one important factor, which can be melt the ink that was firstly printed out on the filter paper and let it penetrate throughout the paper. To compare the result of the influence of heater, hotplate and hot air oven were used to heat the devices because the important difference between hotplate and hot air oven is hotplate cannot completely control temperature when compared with hot air oven, which is the enclose environment heater.

To use both hotplate and hot air oven for optimizing heating temperature and heating time, the heating temperature was ranged from: 165, 180, 190, 200, 220, and 260 °C with the heating time of each temperature: 15, 30, 45 minutes, and 1 hour, respectively.

The results shown that both heaters can melt the laser printer's toner ink at 260 °C with different in time. The hotplate achieved to create hydrophobic barrier on the filter paper after heating the devices for 1 hour to melt the ink, while the hot air oven uses only 15 minutes of heating. The reason that both hotplate and hot air oven achieved to create a hydrophobic barrier on the filter paper is because this temperature corresponds to the melting point of polyester, which is one of hydrophobic components that contain in laser printer's toner ink. Heating the devices with a hot air oven instead of a hotplate can significantly reduce the heating time. This is because the hot air oven is the enclose environment heater, which temperature can be precisely controlled inside the oven, compared with the hotplate that cannot control the environment temperature. So, the accuracy of controlling temperature was higher. However, although the heating time can be reduced by using hot air oven, the heating temperature still too high to heat the devices, which resulted in pyrolysis of the filter paper that causing the paper turns into yellow color.

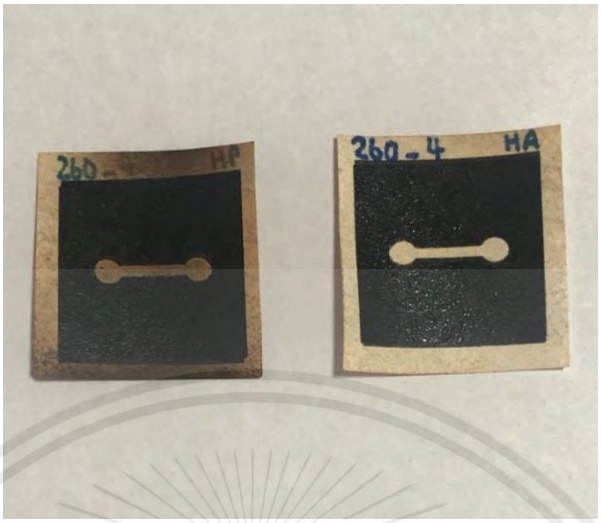

Figure 4-3. The comparison of the color paper which influence from the heater between heating on the hotplate (Left: 1 hour at 260 °C) and heating in the hot air oven (Right: 15 minutes at 260 °C)

To solve the problem of pyrolysis of the paper, the printer was changed to be 'Thermal Transfer Printer'.

4.2.2 Result of Paper-based Microfluidic Devices Fabrication by Thermal Transfer Printer

HPRT MT800 portable A4 Thermal Transfer Printer was used in this project to pattern the hydrophobic barrier on the filter paper. It uses heat to transfer a wax-based solid ink from carbon ribbon onto the filter paper. The main advantage of this printer is the carbon ribbon has a low melting point, which means high heating temperature and long time for heating device are not required. So, the filter paper would not be pyrolyzed by the heater.

4.2.2.1 The resolution of hydrophobic barriers

The resolution of hydrophobic barriers, that were patterned on the filter paper by Thermal Transfer Printer, was relatively low and cause some areas of ink disappear. This is because Thermal Transfer Printer is usually suitable to be used in barcodes and labels printing, but the filter paper has a surface roughness higher than other papers. The resolution of hydrophobic barriers, that was patterned by Thermal Transfer Printer,

can be improved by re-patterning. However, to achieve good alignment of the devices in each time of patterning will be challenging.

In this result, it shown that 2-time patterning has a higher resolution than 1-time patterning, as shown in Figure 4-4. Both 1-time and 2-time patterning achieved to form hydrophobic barrier on the filter paper by containing and transfer the red dye solution along the hydrophilic channel. It can be confirmed that 2-time patterning is sufficient to improve the resolution and form hydrophobic barrier on the filter paper, which was selected for use in the next experiment.

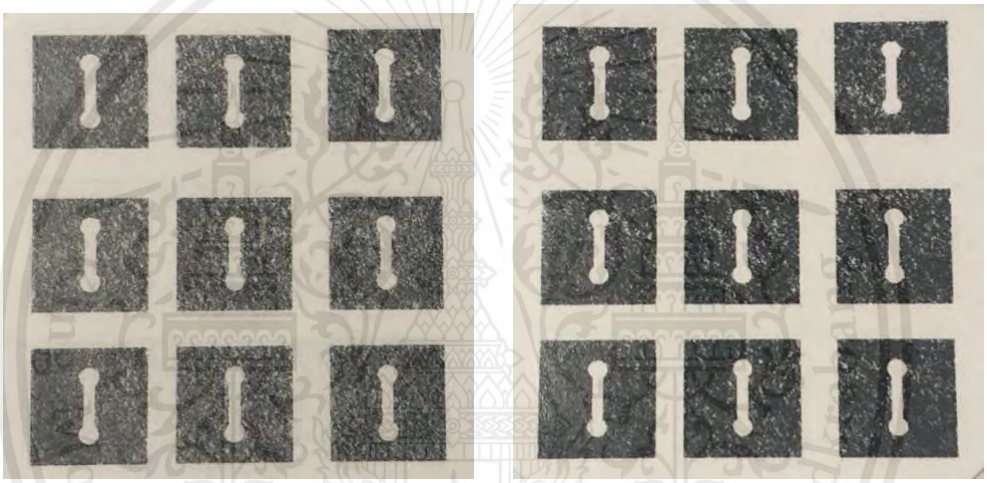

Figure 4-4. The comparison of thermal transfer printer resolution between 1-time patterning (Left) and 2-time patterning (Right)

4.2.2.2 Flow characterization according to Heating Temperature and Heating time

To analyze flow characterization according to heating temperature and heating time, an electric oven was used instead of a hot air oven during the fabrication processes. This decision was persuaded by unexpected issues that I got from the hot air oven, which temperature cannot be controlled, and unstable temperature control caused by malfunctioning in the hot air oven at that time. So, choosing an electric oven for heating the devices instead of a hot air oven is a suitable alternative option because an electric oven is available in the commercial market, cost-effective, and it is an enclosed environment heater that can precisely control temperature similar as a hot air oven.

After heating the devices at each defined heating temperature and heating time, the result shown that at 5 minutes, the heating time was not enough to melt the carbon ribbon and it could not form a hydrophobic barrier on the filter paper, so 5 minutes of heating time would not be considered. While 15 minutes of heating time were enough to melt the carbon ribbon at every defined temperature. The characterization of the device at each defined heating temperature at 15 minutes of heating time shown that at 90, 120, and 150 °C, pyrolysis of the filter paper did not occur, while at 180 °C, the white filter paper turned to brown due to pyrolysis of the paper caused by too high heating temperatures.

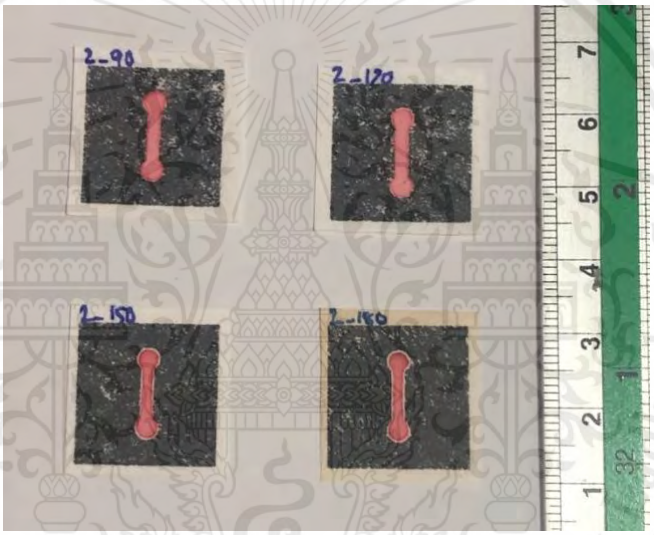

Figure 4-5. The comparison of flow characterization and color paper which influence from the heating temperature and heating time and heated in electric oven for 90 °C, 120 °C, 150 °C, and 180 °C, respectively. (From upper left to lower right)

According to the result of the flow characterization analysis, at 90 °C of heating temperature gave the fastest flow speed of red dye color solution since it was the first to flow and reach at the outlet reservoir, which spent only 12 seconds. while at 120 °C, 150 °C, and 180 °C are the second (30 seconds), third (73 seconds), and fourth (149 seconds) for the speed of flow, respectively. This can be indicated that the flow rate and heating temperature are significantly correlate, which means an increasing in the heating temperature leads to reducing in the flow rate.

4.2.3 Evaluation of the flow rate

4.2.3.1 Optimization of Heating Temperature and Heating Time by considering flow rate

As the result of flow characterization analysis, I found that only 15 minutes of heating time were the heating temperature that achieved to create a hydrophobic barrier on the filter paper and observed that increasing in the heating temperature leads to reducing in the flow rate.

To determine the optimal heating temperature for device fabrication process, the flow characteristic of each defined temperature should be used to compare the flow rate with theoretical equation, which is 'Lucas-Washburn equation', and experimental equation, which is 'A modified Washburn equation' that was derived by Ruiz et. al [27].

The result after plotted the distance of each defined temperature with respect to time against with calculated Lucas-Washburn equation and a modified Washburn equation, graphs of both equations were generated from calculation based on the parameters that was defined in equation which consist of: An average porosity of Double ring 102 filter paper (ϕ) is 8 μm, Surface tension (γ) of flowing liquid solution at room temperature is 0.072 N/m, Contact angle between the capillary wall and liquid (θ) is 30°, Dynamic viscosity of the liquid at room temperature (μ) is 0.00089 $N \cdot s/m^2$, with the time ranging from 0 to 12 seconds in 1 second increment, for Lucas-Washburn equation, and 0 to 100 seconds in 1 second increment of a modified Washburn equation.

From the graph result [Figure 4-6], the relationship between experimental results of each defined temperature and Lucas-Washburn equation were very low and they were inconsistent and not correlate with any heating temperatures. This is because according to Lucas-Washburn equation is not valid for paper channel with the wax boundaries, so the viscous force and reverse surface tension are not accounted in their equation. However, in the reality, the hydrophobic channel boundaries can affect the imbibition dynamics in the channel [28]. Therefore, a modified Washburn equation, that was derived by Hong et al. [28], was used and applied to determine the optimal heating temperature instead. Based on comparing the relationship between experimental results of each defined temperature and a modified Washburn equation, it

can be indicated that a relationship between experimental results of heating temperature at 120 °C and a modified Washburn equation, they got the best correlation when compared with other heating temperatures which has very high relationship and high consistency of distance of liquid solution flowing with respect to time. This is because addition of the viscous force and reverse surface tension in a modified Washburn equation would be helping to calculate the flow characterization through wax boundaries based on the experiment. Finally, for the assumption, the optimal heating temperature is 120 °C with 15 minutes of heating time and a modified Washburn equation can be used to predict the total length of hydrophilic channel in paper-based microfluidic devices with any expect defined times.

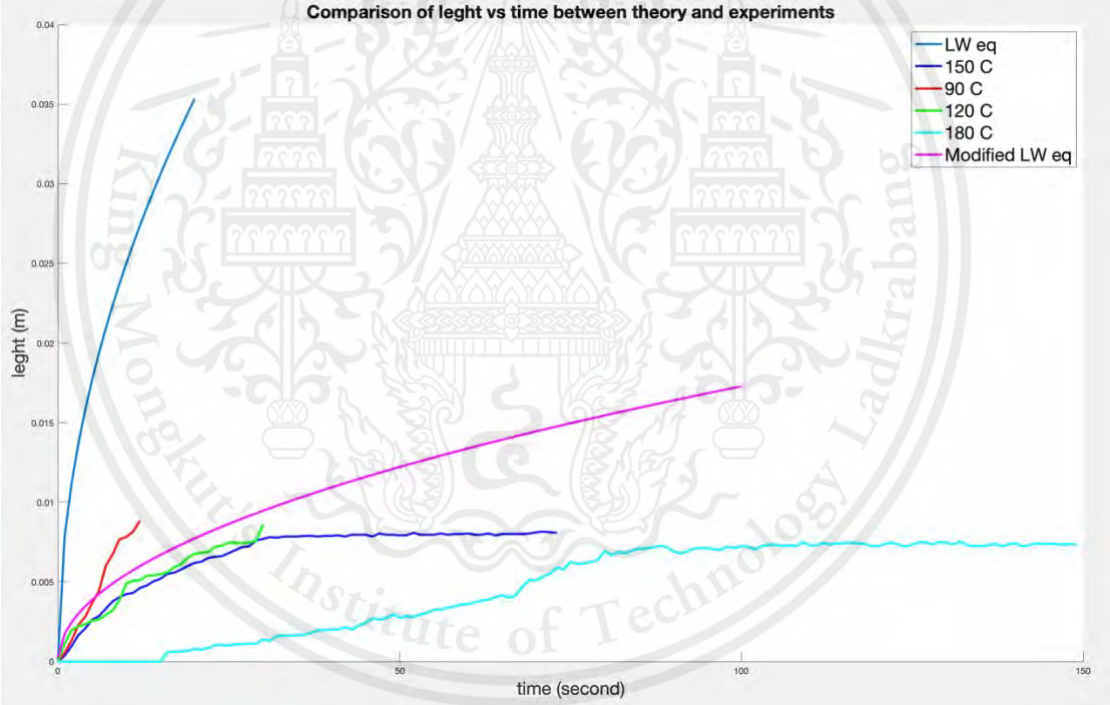

Figure 4-6. The graph of flow length (m) with respect to time (s) compared between experimental results, Lucas Washburn equation, and a modified Washburn equation

4.2.3.2 The influence of the device dimensions on flow rate

After determining the optimal heating temperature and heating time, the 4th and 5th prototype were designed based on the amplification step, which require 30 minutes to amplify the number of samples with amplification reagent. To investigate the

effective hydrophilic channel width to let the red dye color solution flow along the channel, the hydrophilic channel width (w) was varied and defined in a modified Washburn equation to calculate the required hydrophilic channel length (lm) for 30-minute-long. It was observed that the calculated hydrophilic channel length (lm) depends on the hydrophilic channel width (w) where wider channel width is required, the channel length is reduced. 4 hydrophilic channel lengths: 1, 1.5, 2, and 4 mm, were selected to use in this experiment. Then, the devices were patterned for 2 times by Thermal Transfer Printer and heated in an electric oven at 120 °C for 15 minutes.

In the results, after 10 μl increment of red dye color solution was added into sample inlet reservoir of each device, it was observed that, in the design of 1 millimeter in channel width, the red dye solution was unable to flow along the channel. This is due to the design's very narrow hydrophilic channel width. For the designs with channel width of 1.5, 2, and 4 mm, the red dye color solution was able to flow in distance of 1.70, 3.45, and 3.8 cm, respectively, within 30 minutes. The distance of the red dye color solution that flowed along the channel was close to the distance determined by a modified Washburn equation, indicating that 4 mm was the most effective hydrophobic channel width. Nonetheless, for the entire 30 minutes, it was needed to continue keeping checking on the red dye color solution to prevent the solution dry before 30 minutes. It was observed that, the addition of red dye solution in 30 μl, the A4 paper that was used as the device's foundation indicated some leakage of the solution, and the total volume of red dye color solution that was added for entire 30 minutes was 70 μl.

According to this experiment's results, the flow rate is influenced not only by heating temperature but also by the device's characterization, meaning that a narrower channel width resulted in a noticeable decrease in flow speed until it cannot flow in 1 mm of channel width. And based on my assumption about the solution leakage when placed devices on A4 paper, it showed that the flow of red dye color solution was interrupted and inhibited by the contact surface between devices and A4 paper that were placed on a table surface.

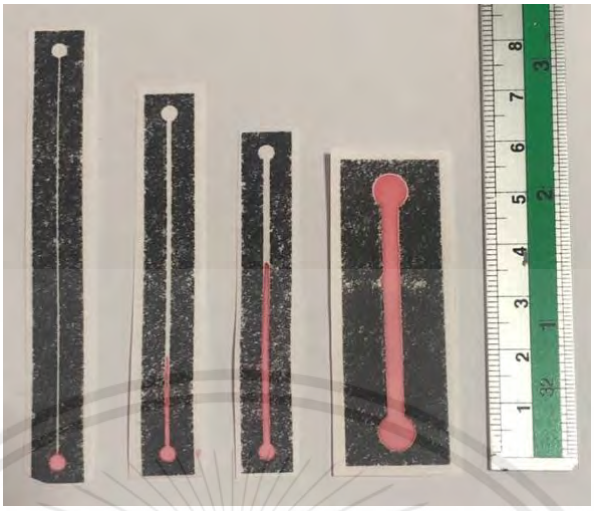

Figure 4-7. A difference in device characterization with respect to the effect of channel width on flow rate (1, 1.5, 2, and 4 mm in channel width, respectively)

4.2.3.3 The Optimal Volume Quantity

Followed by the previous experiment (4.2.3.2), which required to continue checking for an addition of 10 μl increments of red dye color solution for the entire 30 minutes, it could not be shown the exact volume quantity that was required for flowing in 30 minutes, and the result indicated some leakage of the solution from the devices onto A4 paper. To determine the optimal volume quantity for 15-minute and 30-minute flow and investigate the flow behavior on different contact surfaces, the 5^{th} and 6^{th} prototypes were used by placing in different conditions, which placed the devices on A4 paper and suspend in air by using cooling rack, to compare the results. Since, the total volume that was added in previous experiment was 70 μl, so in this experiment the volume quantity was ranged from 30 μl to 70 μl, in 10 μl increment.

After testing the influence of the contact surface on the flow rate, it was indicated that, the devices that were suspended in the air by using cooling rack, the red dye solution could flow with high consistency by the distances of each retesting were quite close together when compared with the devices that were placed on A4 paper. This is because to suspend the devices in the air, the contact surface of either A4 paper or table surface could not interrupt and inhibit the flow of red dye color solution, which means the flow rate was not affect with this factor. However, I observed that fixing the

position of the devices on the cooling rack of each testing could achieve greater consistency than not fixing the position. So, based on these observations, the results of device, that were placed on cooling rack, were only selected to plot the flow rate against a modified Washburn equation for optimizing the volume quantity in each flow time, which are 15 and 30 minutes.

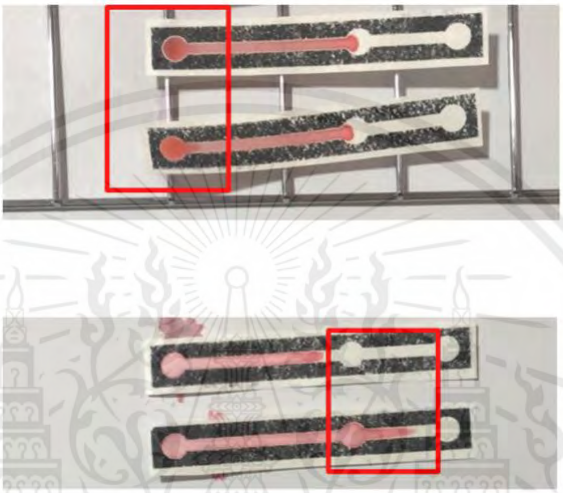

Figure 4-8. The comparative analysis of the effect and consistency of solution flow due to contact surface. This comparison demonstrates the observation when the devices are placed on cooling rack compared with A4 paper.

The results showed that, the optimal volume quantity of 15-minute and 30-minute solution flowing were 40 μl and 30 μl, which can flow 3.99 and 3.48 cm in length, respectively. This is because the flow rate of both volume quantity had the most correlation with a modified Washburn equation of each expected time, as shown in Figure 4-10, 4-12.

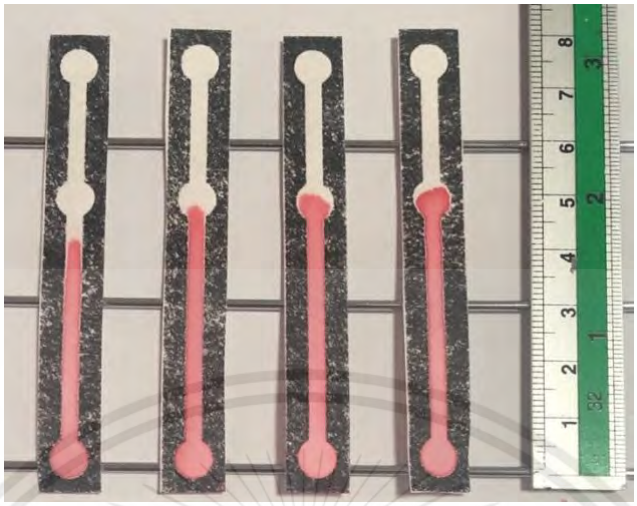

Figure 4-9. The comparative analysis of the different volume quantity (30 μl, 40 μl, 50 μl, 60 μl, respectively) impacted with the solution flow in 30 minutes for amplification step in CRISPR-Cas12a system.

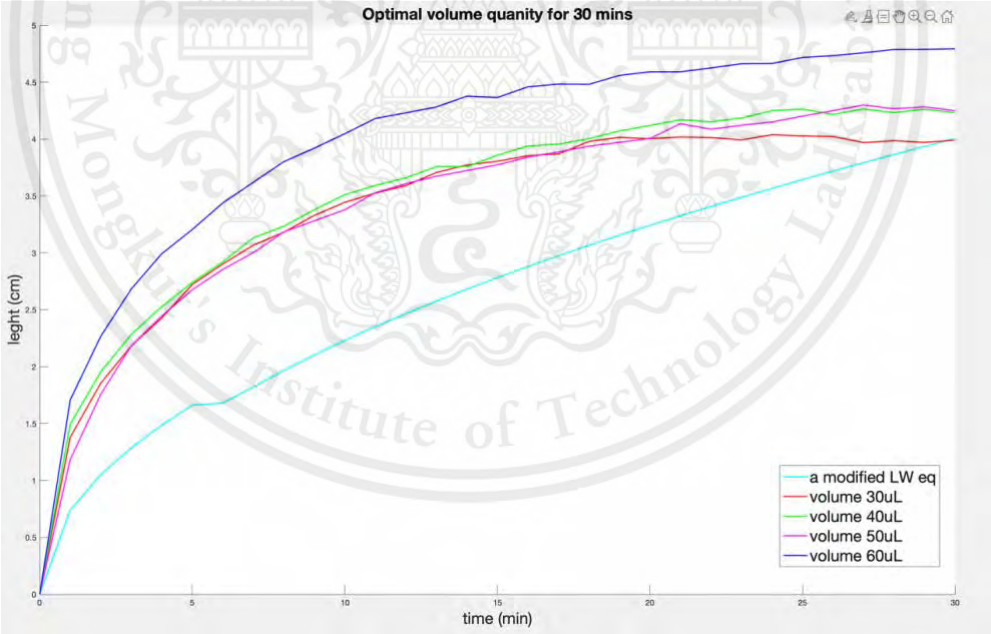

Figure 4-10. The comparative graph analysis of the different volume quantity (30 μl, 40 μl, 50 μl, 60 μl, respectively) impacted with the solution flow in 30 minutes for amplification step in CRISPR-Cas12a system. This graph illustrates the correlation between experimental results of each volume quantity compared with a modified Washburn equation.

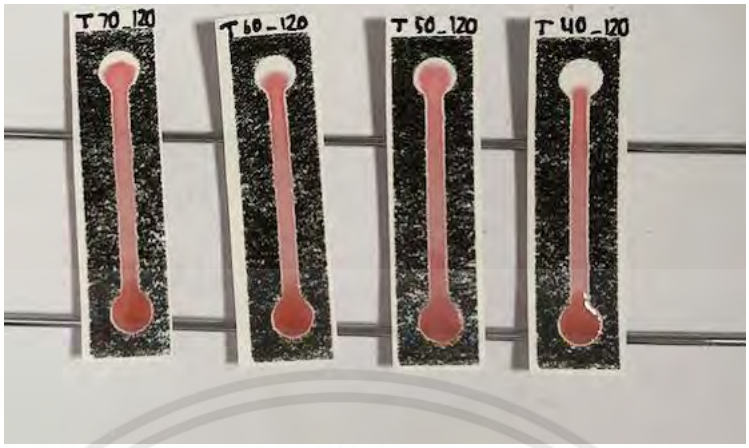

Figure 4-11. The comparative analysis of the different volume quantity (40 μl, 50 μl, 60 μl, 70 μl, respectively) impacted with the solution flow in 15 minutes for detection step in CRISPR-Cas12a system.

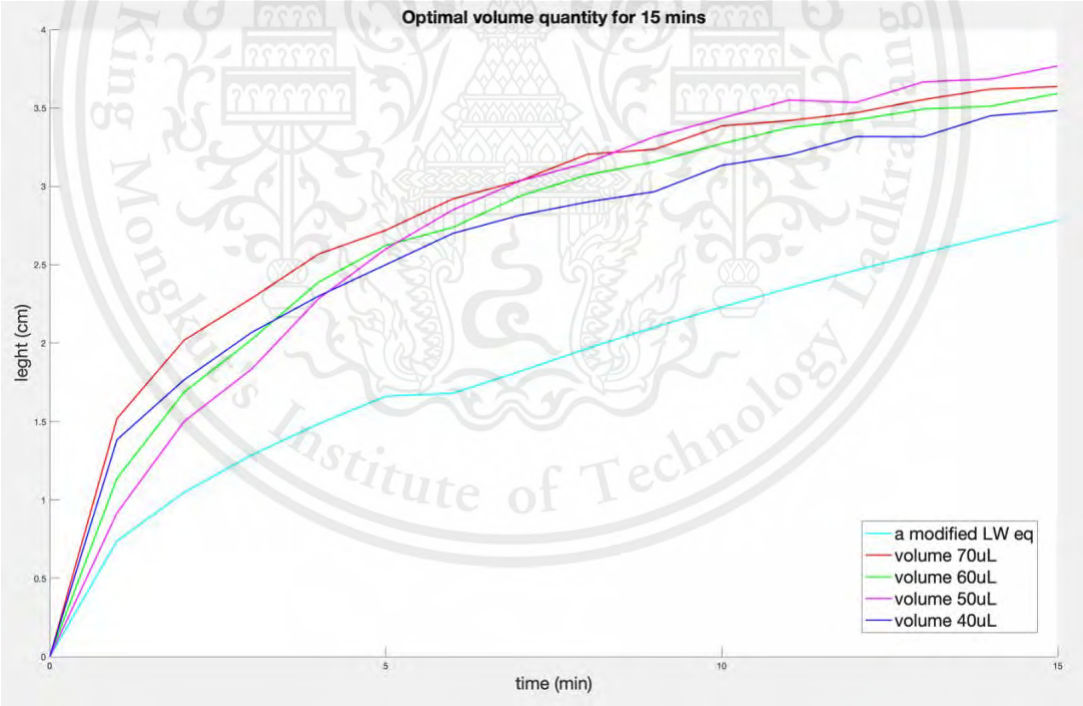

Figure 4-12. The comparative graph analysis of the different volume quantity (40 μl, 50 μl, 60 μl, 70 μl, respectively) impacted with the solution flow in 15 minutes for detection step in CRISPR-Cas12a system. This graph illustrates the correlation between experimental results of each volume quantity compared with a modified Washburn equation.

4.2.4 Effective Mixing on Paper-based Microfluidic Device

Followed by the CRISPR-Cas12a system for COVID-19 Diagnostic from section (2.3.4), 2 main steps of this assay were integrated in the paper-based microfluidic device by separating the sample inlet reservoir of prototype design into 2 reservoirs for adding the RNA sample (or template sequences) and CRISPR reagent. However, after the discussion between my advisor and Chula team about the simplest version of developing paper-based microfluidic device for CRISPR diagnostic of COVID-19, they are agreed to assume that the sample has a high concentration of target DNA enough to ignore and skip the amplification step, which means it is not necessary to concern about the solution flow for 30 minute-long. Although the amplification step can be skipped, the concept design of reservoirs separation between sample and CRISPR reagent still employed because it will increase the ease of use for users to add both sample and CRISPR reagent at the same time and just only wait for the result.

The effective mixing between sample and CRISPR reagent during the flow on the device is another important factor that should be considered because it can be affected with the accuracy and efficiency of the CRISPR reaction. To investigate the most effective mixing design on paper-based microfluidic device by using the concept of passive micromixer which use chaotic advection, the cross-shape design from Weng et al. [32], T-shape and Y-shape designs from Green [35] were used, which is the 7th prototype [Figure 3-7].

Based on the published article from Mayuramart et al. [2] , they showed the setup of sample and CRISPR reagent for using in the detection step as shown in the Table 4-1.

Table 4-1. The CRISPR detection setup

Reagent	Volume (μl)
DEPC-treated water	13.64
NEBuffer 2.0 (New England Biolabs, USA, B7002S)	2
300 nM crRNA	2
1 μM EnGen Lba Cas12a (Cpf1) (New England Biolabs, USA, M0653T)	0.66
15 μM 6-FAM	0.66
Amplified template	1
Total	20

To demonstrate the experiment based on this setup, the DEPC-treated water was divided for making the volume of both sample (Amplified template) and CRISPR reagent (NEBuffer, crRNA, Cas12, 6-FAM) reservoirs equally to let the flow reach the mixing channel at the same time. For each ratio of volume divisions between sample : CRISPR reagent were shown in Table 4-2, 4-3, 4-4.

Table 4-2. The CRISPR detection setup with the ratio 20 μl sample reservoir : 20 μl CRISPR reservoir

Reagents	**20 μl : 20 μl**	
	Sample reservoir	**CRISPR reservoir**
DEPC-treated water	18 uL	9.28 uL
NEBuffer 2.0 (New England Biolabs, USA, B7002S)	-	4 uL
300 nM crRNA	-	4 uL
1 μM EnGen Lba Cas12a (Cpf1) (New England Biolabs, USA, M0653T)	-	1.32 uL
15uM 6-FAM	-	1.32 uL
Amplified templated	2 uL	-
Total	20 uL	20 uL

Table 4-3. The CRISPR detection setup with the ratio 40 μl sample reservoir : 40 μl CRISPR reservoir

Reagents	**40 μl : 40 μl**	
	Sample reservoir	**CRISPR reservoir**
DEPC-treated water	36 uL	18.56 uL
NEBuffer 2.0 (New England Biolabs, USA, B7002S)	-	8 uL
300 nM crRNA	-	8 uL
1 μM EnGen Lba Cas12a (Cpf1) (New England Biolabs, USA, M0653T)	-	2.64 uL
15uM 6-FAM	-	2.64 uL
Amplified templated	4 uL	-
Total	40 uL	40 uL

Table 4-4. The CRISPR detection setup with the ratio 60 μl sample reservoir : 60 μl CRISPR reservoir

Reagents	**60 μl : 60 μl**	
	Sample reservoir	**CRISPR reservoir**
DEPC-treated water	54 uL	27.84 uL
NEBuffer 2.0 (New England Biolabs, USA, B7002S)	-	12 uL
300 nM crRNA	-	12 uL
1 μM EnGen Lba Cas12a (Cpf1) (New England Biolabs, USA, M0653T)	-	3.96 uL
15uM 6-FAM	-	3.96 uL
Amplified templated	6	-
Total	60 uL	60 uL

The ratio of 40 μl : 40 μl and 60 μl : 60 μl were selected to use for observing the mixing efficiency of each device design in the experiment of including temperature control. This is because the ratio of 20 μl : 20 μl is too less for flowing on the device when the temperature was controlled at 37 °C.

4.2.4.1 Excluding Temperature Control

In this experiment, the yellow and blue dye solution were used instead of the real sample and CRISPR reagent to observe the mixing efficiency between 3 designs of device, which are cross-shape, Y-shape, and T-shape design.

To fabricate the devices, the devices were patterned by printing from Thermal Transfer Printer only one time. Although the resolution of 2-time patterning higher than 1-time patterning and enhance the hydrophobicity of the barrier, to repattern the complex design will be challenging and difficult to get the complete alignment of the design. However, although the resolution of 1-time patterning is not high as 2-time patterning, it is sufficient to create the hydrophobic barrier. The length of hydrophilic mixing channel of all designs were defined based on the experiment of solution flow within 15 minutes in section (3.4.3), which is equal 3.48 cm.

After both yellow and blue dye solution were added into each inlet reservoirs with different ratio, the time was recorded when both yellow and blue dye solution was starting mix together in mixing channel. The results showed that the mixing solution in all designs able to flow along the mixing channel and reach to the outlet reservoir within 15 minutes, as shown in Figure 4-13.

Figure 4-13. The effective design for sample mixing in microchannel analyzed in cross-shape, T-shape, and Y-shape designs by excluding the temperature control.

According to analyze the most effective mixing design for paper-based microfluidic device, the hydrophilic mixing channel was separated into 7 areas for observing the Hue range within each area and compared it with the reference, which is from the Hue range of green solution that mixed by yellow and blue dye solution in equal of ratio. After careful consideration, the percentage of error for the Hue range that acceptable is 20%.

The result of this experiment indicated that the most effective design for mixing between yellow and blue dye solutions is 'cross-shape' design. The cross-shape design achieved a mixing efficiency reaching up to 20% of the acceptable Hue range at 3rd area (Green_3). It showed successful mixing of both yellow and blue dye solution from 3rd area onward. In the other hand, the T-shape design achieved a 20% of acceptable Hue range at the 7th area (Green_7), while the Y-shape did not reach that range, as show in the Table 4-5.

Table 4-5. The summary of Hue range for each area

Area	Cross-shape	T-shape	Y-shape	Reference
Yellow	-	-		37-39
Blue	-	-		145-165
Green_1	54-92	38-46	33-38	66-69
Green_2	50-65	42-50	22-36	-
Green_3	52-68	43-48	20-32	-
Green_4	55-70	36-39	20-34	-
Green_5	59-63	38-44	54-112	-
Green_6	65-71	35-44	60-110	-
Green_7	74-76	62-67	80-107	-
20% error	-	-	-	52.8-82.8
30% error	-	-	-	46.2-89.7
40% error	-	-	-	39.6-96.7
50% error	-	-	-	33-103.5

The reason that the cross-shape design can mix both dye solutions better than the T-shape and Y-shape is because the only parallel flow direction, such as T-shape and Y-shape, is insufficient for mixing the solution. The capillary force, which drive both solution flow along the channel, is insufficient to occur the interaction between

different solutions and let it mix together at the short length of flow. However, the addition of chaotic advection by changing the geometry of the mixing channel can significantly improve the mixing performance, which occurred by the effect of molecular diffusivity [04].

4.2.4.2 Including Temperature Control

Based on the Cas reaction for fluorescent visualization of detection step required to incubate the reaction for 15 minutes at 39 °C [2], the hotplate was used to control the environment temperature while both yellow and blue dye solutions were mixing and flowing along the devices.

The results indicated that both of volume ratio could not flow along the mixing channel until reached the outlet reservoir like the previous test except T-shape design, as shown in the Figure 4-14.

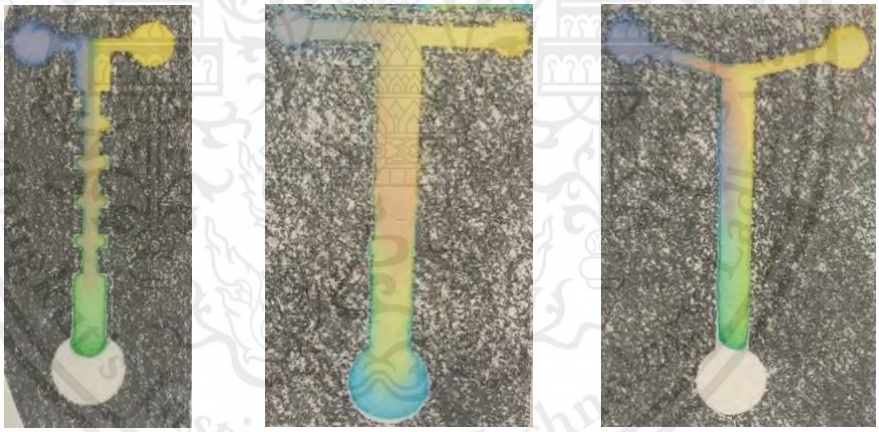

Figure 4-14. The effective design for sample mixing in microchannel analyzed in cross-shape, T-shape, and Y-shape designs by including the temperature control.

This is because the set-controlled temperature was increased and higher than the room temperature. Consequently, the solution was prone to evaporation during its flow that reduced the volume of solution to flow along the mixing channel. Moreover, the temperature of hotplate has 1% margins of error. It was observed that at the center of hotplate has a higher temperature than at the corner, which affected with the flow of solution. Based on this effect, the temperature of hotplate was reduced to be 37 °C

instead and it was assumed that at the center of hotplate will be the most accuracy area to control the environment temperature of the Cas reaction.

Following the Cas reaction, which required 15 minutes for incubation, it is essential to ensure the well mixed of both sample and CRISPR reagent should be considered before commencing the time for the Cas reaction. According to the Table 4-5, the most effective design for mixing solutions is the cross-shape design and achieved a mixing efficiency reaching up to 20% of the acceptable Hue range at the 3rd area (Green_3). Therefore, the initiation to account the time for the Cas reaction should start when the mixing solution flow to the 3rd area (Green_3).

Subsequently, the mixing efficiency of both volume ratios were relatively similar, which the mixing efficiency will be improved after from the 3rd area (Green_3) onwards. Although the volume of 60 μl : 60 μl ratio have a higher volume than 40 μl : 40 μl ratio, the flow length on the mixing channel of both ratios still relatively the same. This is due to the limitation of paper's porosity that limited by the hydrophobic barrier, which restricting the volume of solutions that can flow through the mixing channel and constraining the volume of solution per area of mixing channel. Moreover, based on my observation, it indicated that the consistency in the flow length of the 60 μl : 60 μl volume ratio was lower than the 40 μl : 40 μl ratio. This is due to the 60 μl of volume was excessive for containing on the sample inlet reservoir, causing the solution to penetrate through the sample inlet reservoir and form a solution meniscus underneath reservoir, which reducing and hindering the flow of solution on the device.

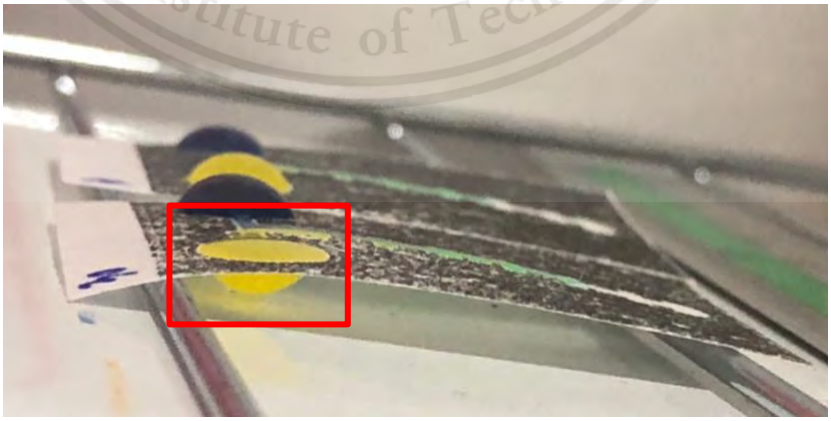

Figure 4-15. A 60 μl solution meniscus underneath reservoir

As was mentioned previously, it can be indicated that to control the volume ratio for flowing along the mixing channel to the outlet reservoir has more difficulty than adjusting the mixing channel length. So, the volume ratio of 40 μl : 40 μl was selected to use for observing the average flow length of mixing solution along the mixing channel. The experimental results showed that the average flow length of mixing solution along the mixing channel was equal 2.74 cm, as shown in Table 4-6.

Table 4-6. The average flow length of 40 μl for 6 tests

Testing	**Flow length of 40 μl**
1	2.748
2	2.747
3	2.499
4	2.709
5	2.786
6	2.925
Average	2.735

After determining the mixing channel length based on the experimental results, the last prototype [Figure 3-8] was designed by increasing the length via AutoCAD 2023 program to be 30 mm due to the patterns, that were printed by Thermal Transfer Printer, were scaled down to 94.2% [27] and the exact length of mixing channel after printed out was equal 28 mm. In order to test the consistency of the solution flow along the device, the experiment was reconducted for 10 times. The results indicated that the average flow lengths of mixing solution were reduced to be 2.55 cm. However, when compared the flow length of each test with the theory, which is calculated from a modified Washburn equation, the difference of flow length is not lower than 20% of the theory flow length. Finally, it was observed that the percentage of reproducibility of this experiment was 70%, which the mixing solution success to flow along the mixing channel followed by all required conditions as shown in Table 4-7.

Table 4-7. The average flow length, percentage of flow length, and percentage of reproducibility of 40 μl for 10 tests

Testing	Flow length of 40 uL	% of flow length compared with Theory length
1	2.69	93.42%
2	2.607	90.53%
3	2.472	85.85%
4	2.507	87.06%
5	2.568	89.19%
6	2.346	81.48%
7	2.371	82.34%
8	2.531	87.90%
9	2.619	90.95%
10	2.771	96.24%
Average	2.5482	88.50%
Theory	2.8794	100%
Reproducible	success 7 from 10	70%

4.3 Chapter Summary

This chapter exemplifies successful fabrication processes in achieving the optimal conditions for producing paper-based microfluidic devices and compatible with the CRISPR-Cas12a concept. To fabricate paper-based microfluidic devices with an optimal condition, thermal transfer printer was used to pattern the hydrophobic barrier on the Double Ring 102 filter paper, followed by heating in an electric oven at 120 °C of the heating temperature with 15 minutes of the heating time. However, integrating the CRISPR-Cas12a assay into a paper-based microfluidic device needs to consider about the effective mixing between sample and CRISPR reagent. To enhance the mixing efficiency on paper-based microfluidic devices, the cross-shape design was used, offering to be the most effective design in comparison to T-shape and Y-shape designs. This experiment was made through the Hue range of color analysis via an ImageJ program for observation of mixing color between 40 μl of yellow dye solution and 40 μl of blue dye. The tests were conducted 10 times to observe the consistency of solution flow, mixing efficiency, and percentage of producibility. The results indicated that the cross-shape design success to improve the mixing efficiency by reaching up to

20% of the acceptable Hue range at the 3rd area (Green_3) section for all tests, the average flow length is 2.5482 cm, which is approximately 88.50% compared with the flow length that calculated from a modified Washburn equation, and the percentage of reproducibility is 70%. Additional information for each test is detailed in the appendix section.

CHAPTER 5
CONCLUSION

5.1 Introduction

This chapter provides a summary of the key processes of entire project from chapter 1 until chapter 5 (section 5.2), conclusion of the entire key concepts and results that we have done during this project (section 5.3), and also mentioned about the future work and future plan to complete the remaining part of this project within next year (section 5.4).

5.2 Summary

In summary, COVID-19 is an infectious disease that caused by the SAR-CoV-2 and infected from person-to-person around the world. Currently, the gold standard for COVID-19 detection is RT-PCR. However, it requires a high cost of test and time consuming. So, ATK is developed to reduce the detection time and increase ease of use, but the sensitivity of this methods is only 49%. CRISPR-Cas12a system is developed to be a new alternative detection method, which provides a high sensitivity and specificity as RT-PCR, but easy to use and time saving as ATK. However, the multiple steps of CRISPR-Cas12a system in the laboratory is difficult to perform with everyone use and it can be reduced the ease of use.

So, our objective during this project is successfully apply the CRISPR-Cas12a system into paper-based microfluidic device for using as a POC diagnostic and observe the optimal conditions and device characteristics for CRISPR-Cas12a diagnostic to increase the ease of use which can be accessed with everyone, improve the sensitivity and specificity, low cost producing, and time saving. During the project, 8 prototype designs were used to test with total 9 experiments as detailed in the chapter 3. All results of each experiment provide in the chapter 4, and they were included in the chapter 5 (section 5.3).

5.3 Conclusions

This project successfully fabricated the paper-based microfluidic devices with the best and optimal conditions for combining with the CRISPR-Cas12a system owing to the COVID-19 or any infectious disease detection. The paper-based microfluidic devices were easily fabricated by Thermal Transfer Printer and melt the ribbon carbon by heating in electric oven for 15 minutes at 120 °C. These optimal conditions were concerned by observing consistency based on a modified Washburn equation from Hong. et al. [28], which derived the experimental equation from the Lucas Washburn equation.

To integrate the concept of CRISPR-Cas12a system into the paper-based microfluidic devices, this project started with the simplest idea which assumed that the sample has a high concentration of target DNA enough to skip the amplification step (30 minutes) and only focus on the CRISPR reaction for detection step (15 minutes). The cross-shape design of 8^{th} prototype successfully to use as a micromixer for the most effective design of sample mixing in microchannel. The experimental results indicated that at the area 3 (Green_3), the Hue value was improved and increased to reach at 20% of acceptable Hue range of green color (Reference). Based on [Table 6], it can be shown that the cross-shape design has a high ability to mix the reagent on the paper-based microfluidic devices by do not require the additional external pump because the cross-shape design provided more chaotic advection by designing the complicated geometric of mixing channel to improve the mixing efficiency rather than using only parallel flow direction like T-shape and Y-shape designs. The average flow length of mixing solution, after reached at 20% of acceptable Hue range of green color (Reference), is 2.55 cm, which approximately 88.50% compared with the calculated flow length from a modified Washburn equation (Theory). The percentage of reproducibility is 70% [Table 4-7]. Additionally, the other experimental results of 10 tests in section 4.2 are provided and detailed in the Appendix A, while the tables of frequency distribution of Hue value are provided and detailed in the Appendix B.

5.4 Future Work

The duration of this project is expected to be succussed and completed within the next year. The short plan of this project is to continue optimizing the best condition of paper-based microfluidic devices for applying with the CRISPR-Cas12a assay and use the real sample of target sequence (DNA with a high concentration) and CRISPR reagent set up, as shown in Table 4. The long-term plan of this project is to incorporate the positive control in the prototype design for checking the sample and CRISPR reagent during testing the result on the paper-based microfluidic devices.

REFERENCES

[1] J. P. Broughton *et al.*, "CRISPR–Cas12-based detection of SARS-CoV-2," *Nat Biotechnol*, vol. 38, no. 7, pp. 870–874, Jul. 2020, doi: 10.1038/s41587-020-0513-4.

[2] O. Mayuramart *et al.*, "Detection of severe acute respiratory syndrome coronavirus 2 and influenza viruses based on CRISPR-Cas12a," *Exp Biol Med (Maywood)*, vol. 246, no. 4, pp. 400–405, Feb. 2021, doi: 10.1177/1535370220963793.

[3] "Thailand: WHO Coronavirus Disease (COVID-19) Dashboard With Vaccination Data." Accessed: Nov. 03, 2023. [Online]. Available: https://covid19.who.int

[4] M. Issarasongkhram, "The study of sensitivity, specificity and accuracy of Antigen Test Kits (ATK) compare with Real time RT-PCR for Coronavirus 2019 at Coronavirus 2019's field screening service, Bangkok", *IUDCJ*, vol. 6, no. 2, pp. 101–111, Feb. 2022.

[5] B. Hu, H. Guo, P. Zhou, and Z.-L. Shi, "Characteristics of SARS-CoV-2 and COVID-19," *Nat Rev Microbiol*, vol. 19, no. 3, pp. 141–154, Mar. 2021, doi: 10.1038/s41579-020-00459-7.

[6] Y. Yang *et al.*, "SARS-CoV-2: characteristics and current advances in research," *Virol J*, vol. 17, no. 1, p. 117, Dec. 2020, doi: 10.1186/s12985-020-01369-z.

[7] V. Ravi, S. Saxena, and P. S. Panda, "Basic virology of SARS-CoV 2," *Indian Journal of Medical Microbiology*, vol. 40, no. 2, pp. 182–186, Apr. 2022, doi: 10.1016/j.ijmmb.2022.02.005.

[8] K. Dhama *et al.*, "Coronavirus Disease 2019–COVID-19," *Clin Microbiol Rev*, vol. 33, no. 4, pp. e00028-20, Sep. 2020, doi: 10.1128/CMR.00028-20.

[9] P. V'kovski, A. Kratzel, S. Steiner, H. Stalder, and V. Thiel, "Coronavirus biology and replication: implications for SARS-CoV-2," *Nat Rev Microbiol*, vol. 19, no. 3, pp. 155–170, Mar. 2021, doi: 10.1038/s41579-020-00468-6.

[10] H. Su, Y. Xu, and H. Jiang, "Drug discovery and development targeting the life cycle of SARS-CoV-2," *Fundamental Research*, vol. 1, no. 2, pp. 151–165, Mar. 2021, doi: 10.1016/j.fmre.2021.01.013.

[11] O. Filchakova, D. Dossym, A. Ilyas, T. Kuanysheva, A. Abdizhamil, and R. Bukasov, "Review of COVID-19 testing and diagnostic methods," *Talanta*, vol. 244, p. 123409, Jul. 2022, doi: 10.1016/j.talanta.2022.123409.

[12] G. Popov, O. Nakov, and A. Popova, "Improving the Accuracy of Rapid Antigen Tests for Covid-19 using Data Mining and Blood Test," in *2022 10th International Scientific Conference on Computer Science (COMSCI)*, Sofia, Bulgaria: IEEE, May 2022, pp. 1–4. doi: 10.1109/COMSCI55378.2022.9912572.

[13] D. Đermić *et al.*, "Reverse transcription-quantitative PCR (RT-qPCR) without the need for prior removal of DNA," *Sci Rep*, vol. 13, no. 1, p. 11470, Jul. 2023, doi: 10.1038/s41598-023-38383-4.

[14] G. Rong, Y. Zheng, Y. Chen, Y. Zhang, P. Zhu, and M. Sawan, "COVID-19 Diagnostic Methods and Detection Techniques," in *Encyclopedia of Sensors and Biosensors*, Elsevier, 2023, pp. 17–32. doi: 10.1016/B978-0-12-822548-6.00080-7.

[15] W.-Y. Hsieh *et al.*, "Development and Efficacy of Lateral Flow Point-of-Care Testing Devices for Rapid and Mass COVID-19 Diagnosis by the Detections of SARS-CoV-2 Antigen and Anti-SARS-CoV-2 Antibodies," *Diagnostics*, vol. 11, no. 10, p. 1760, Sep. 2021, doi: 10.3390/diagnostics11101760.

[16] H. Rahimi *et al.*, "CRISPR Systems for COVID-19 Diagnosis," *ACS Sens.*, vol. 6, no. 4, pp. 1430–1445, Apr. 2021, doi: 10.1021/acssensors.0c02312.

[17] Z. Mao *et al.*, "CRISPR/Cas12a-based technology: A powerful tool for biosensing in food safety," *Trends in Food Science & Technology*, vol. 122, pp. 211–222, Apr. 2022, doi: 10.1016/j.tifs.2022.02.030.

[18] Y. Xu and Z. Li, "CRISPR-Cas systems: Overview, innovations and applications in human disease research and gene therapy," *Computational and Structural Biotechnology Journal*, vol. 18, pp. 2401–2415, 2020, doi: 10.1016/j.csbj.2020.08.031.

[19] A. Samacoits *et al.*, "Machine Learning-Driven and Smartphone-Based Fluorescence Detection for CRISPR Diagnostic of SARS-CoV-2," *ACS Omega*, vol. 6, no. 4, pp. 2727–2733, Feb. 2021, doi: 10.1021/acsomega.0c04929.

[20] T. Zhang *et al.*, "Research Progress and Future Trends of Microfluidic Paper-Based Analytical Devices in In-Vitro Diagnosis," *Biosensors*, vol. 12, no. 7, p. 485, Jul. 2022, doi: 10.3390/bios12070485.

[21] Anushka, A. Bandopadhyay, and P. K. Das, "Paper based microfluidic devices: a review of fabrication techniques and applications," *Eur. Phys. J. Spec. Top.*, vol. 232, no. 6, pp. 781–815, Jun. 2023, doi: 10.1140/epjs/s11734-022-00727-y.

[22] E. Noviana *et al.*, "Microfluidic Paper-Based Analytical Devices: From Design to Applications," *Chem. Rev.*, vol. 121, no. 19, pp. 11835–11885, Oct. 2021, doi: 10.1021/acs.chemrev.0c01335.

[23] X. Li, D. R. Ballerini, and W. Shen, "A perspective on paper-based microfluidics: Current status and future trends," *Biomicrofluidics*, vol. 6, no. 1, p. 011301, Mar. 2012, doi: 10.1063/1.3687398.

[24] S. Kumar, P. Bhushan, A. K. Agarwal, and S. Bhattacharya, "A Historical Perspective on Paper Microfluidic Based Point-of-Care Diagnostics," in *Paper Microfluidics*, S. Bhattacharya, S. Kumar, and A. K. Agarwal, Eds., in Advanced Functional Materials and Sensors. , Singapore: Springer Singapore, 2019, pp. 1–5. doi: 10.1007/978-981-15-0489-1_1.

[25] R. Ghosh, S. Gopalakrishnan, R. Savitha, T. Renganathan, and S. Pushpavanam, "Fabrication of laser printed microfluidic paper-based analytical devices (LP-µPADs) for point-of-care applications," *Sci Rep*, vol. 9, no. 1, p. 7896, May 2019, doi: 10.1038/s41598-019-44455-1.

[26] S. Nishat, A. T. Jafry, A. W. Martinez, and F. R. Awan, "Paper-based microfluidics: Simplified fabrication and assay methods," *Sensors and Actuators B: Chemical*, vol. 336, p. 129681, Jun. 2021, doi: 10.1016/j.snb.2021.129681.

[27] R. A. Ruiz, J. L. Gonzalez, M. Vazquez-Alvarado, N. W. Martinez, and A. W. Martinez, "Beyond Wax Printing: Fabrication of Paper-Based Microfluidic Devices Using a Thermal Transfer Printer," *Anal. Chem.*, vol. 94, no. 25, pp. 8833–8837, Jun. 2022, doi: 10.1021/acs.analchem.2c01534.

[28] S. Hong and W. Kim, "Dynamics of water imbibition through paper channels with wax boundaries," *Microfluid Nanofluid*, vol. 19, no. 4, pp.

845–853, Oct. 2015, doi: 10.1007/s10404-015-1611-3.

[29] M. M. Gong and D. Sinton, “Turning the Page: Advancing Paper-Based Microfluidics for Broad Diagnostic Application,” *Chem. Rev.*, vol. 117, no. 12, pp. 8447–8480, Jun. 2017, doi: 10.1021/acs.chemrev.7b00024.

[30] G. Kunti, S. S. Das, V. M. Pedireddi, A. Bhattacharya, and S. Chakraborty, “Energy-Efficient Micromixing in Paper Based Devices Mediated by the Interplay of Electrical and Thermal Fields”, doi: https://doi.org/10.48550/arXiv.1905.06972.

[31] A. R. Rezk, A. Qi, J. R. Friend, W. H. Li, and L. Y. Yeo, “Uniform mixing in paper-based microfluidic systems using surface acoustic waves,” *Lab Chip*, vol. 12, no. 4, pp. 773–779, 2012, doi: 10.1039/C2LC21065G.

[32] C.-H. Weng, P.-P. Hsu, A.-Y. Huang, and J.-L. Lin, “Paper-Based Microfluidics Perform Mixing Effects by Utilizing Planar Constricted–Expanded Structures to Enhance Chaotic Advection,” *Sensors*, vol. 22, no. 3, p. 1028, Jan. 2022, doi: 10.3390/s22031028.

[33] I. Jang, D. B. Carrão, R. F. Menger, A. R. Moraes De Oliveira, and C. S. Henry, “Pump-Free Microfluidic Rapid Mixer Combined with a Paper-Based Channel,” *ACS Sens.*, vol. 5, no. 7, pp. 2230–2238, Jul. 2020, doi: 10.1021/acssensors.0c00937.

[34] G. Tang, S. Liu, I. Fujino, C. Claramunt, Y. Wang, and S. Men, “H-YOLO: A Single-Shot Ship Detection Approach Based on Region of Interest Preselected Network,” *Remote Sensing*, vol. 12, no. 24, p. 4192, Dec. 2020, doi: 10.3390/rs12244192.

[35] H. C. Green, “Improving Paper-Based Microfluidic Mixing With the Incorporation of Flow Disrupting Structures”.

APPENDIX A

Table of Hue value of each mixing area of each test

Table A-1. The summary table of 1st test analyzing the Hue value for 40 μl : 40 μl of cross-shape design.

	Reference	Cross_40ul_test1				
		Mode	STD	AVG	Max-Min	Range
Blue	150.99	-	-	150.31	-	-
Yellow	35.36	-	-	37.52	-	-
Green_1	AVG: 57.39	51	30.19	79.67	92	51-143
Green_2	Range: 54-63	51	30.19	79.67	92	51-143
Green_3	-	60	5.46	66.72	18	60-78
Green_4	-	60	5.46	66.72	18	60-78
Green_5	-	60	5.46	66.72	18	60-78
20% error	45.92-68.87	-	-	-	-	-
30% error	40.18-74.61	-	-	-	-	-
40% error	34.43-80.35	-	-	-	-	-
50% error	28.69-86.09	-	-	-	-	-

Table A-2. The summary table of 2nd test analyzing the Hue value for 40 μl : 40 μl of cross-shape design.

	Reference	Cross_40ul_test2				
		Mode	STD	AVG	Max-Min	Range
Blue	150.99	-	-	157.51	-	-
Yellow	35.36	-	-	36.73	-	-
Green_1	AVG: 57.39	49	38.89	82.09	101	42-143
Green_2	Range: 54-63	49	14.66	64.77	45	48-93
Green_3	-	54	7.2	58.09	40	42-82
Green_4	-	54	10.12	65	30	53-83
Green_5	-	79	5.9	83.8	22	77-99
20% error	45.92-68.87	-	-	-	-	-
30% error	40.18-74.61	-	-	-	-	-
40% error	34.43-80.35	-	-	-	-	-
50% error	28.69-86.09	-	-	-	-	-

Table A-3. The summary table of 3rd test analyzing the Hue value for 40 μl : 40 μl of cross-shape design.

	Reference	Cross_40ul_test3				
		Mode	STD	AVG	Max-Min	Range
Blue	150.99	-	-	157.51	-	-
Yellow	35.36	-	-	36.73	-	-
Green_1	AVG: 57.39	45	26.83	82.09	101	42-143
Green_2	Range: 54-63	49	14.66	64.77	45	48-93
Green_3	-	54	7.2	58.09	40	42-82
Green_4	-	54	10.12	65	30	53-83
Green_5	-	79	5.9	83.8	22	77-99
20% error	45.92-68.87	-	-	-	-	-
30% error	40.18-74.61	-	-	-	-	-
40% error	34.43-80.35	-	-	-	-	-
50% error	28.69-86.09	-	-	-	-	-

Table A-4. The summary table of 4th test analyzing the Hue value for 40 μl : 40 μl of cross-shape design.

	Reference	Cross_40ul_test4				
		Mode	STD	AVG	Max-Min	Range
Blue	150.99	-	-	156.29	-	-
Yellow	35.36	-	-	36.58	-	-
Green_1	AVG: 57.39	45	26.83	68	83	44-127
Green_2	Range: 54-63	49	8.67	54.65	27	48-75
Green_3	-	49	6.11	53.2	21	47-68
Green_4	-	59	4.44	60.46	17	56-73
Green_5	-	66	1.06	66.42	6.8	64.2-71
20% error	45.92-68.87	-	-	-	-	-
30% error	40.18-74.61	-	-	-	-	-
40% error	34.43-80.35	-	-	-	-	-
50% error	28.69-86.09	-	-	-	-	-

Table A-5. The summary table of 5th test analyzing the Hue value for 40 μl : 40 μl of cross-shape design.

	Reference	Cross_40ul_test5				
		Mode	STD	AVG	Max-Min	Range
Blue	150.99	-	-	152.94	-	-
Yellow	35.36	-	-	37.04	-	-
Green_1	AVG: 57.39	40	19.71	57.93	53	40-93
Green_2	Range: 54-63	43	8.62	51.76	22	43-65
Green_3	-	49	4.59	52.02	19	46-65
Green_4	-	49	4.59	52.02	19	46-65
Green_5	-	67	3.77	68.39	16	65-81
20% error	45.92-68.87	-	-	-	-	-
30% error	40.18-74.61	-	-	-	-	-
40% error	34.43-80.35	-	-	-	-	-
50% error	28.69-86.09	-	-	-	-	-

Table A-6. The summary table of 6th test analyzing the Hue value for 40 μl : 40 μl of cross-shape design

	Reference	Cross_40ul_test6				
		Mode	STD	AVG	Max-Min	Range
Blue	150.99	-	-	148.33	-	-
Yellow	35.36	-	-	37.04	-	-
Green_1	AVG: 57.39	103	25.89	62.2	72	41-113
Green_2	Range: 54-63	49	3.56	49.75	16	46-62
Green_3	-	52	3.63	52.3	14	46-60
Green_4	-	64	3.31	66.19	13	63-76
Green_5	-	69	2.85	71.22	13	68-81
20% error	45.92-68.87	-	-	-	-	-
30% error	40.18-74.61	-	-	-	-	-
40% error	34.43-80.35	-	-	-	-	-
50% error	28.69-86.09	-	-	-	-	-

Table A-7. The summary table of 7th test analyzing the Hue value for 40 μl : 40 μl of cross-shape design

	Reference	Cross_40ul_test7				
		Mode	STD	AVG	Max-Min	Range
Blue	150.99	-	-	151.22	-	-
Yellow	35.36	-	-	37.13	-	-
Green_1	AVG: 57.39	42	18.06	57.07	55	41-96
Green_2	Range: 54-63	42	18.06	57.07	55	41-96
Green_3	-	49	3.31	51.6	11	49-60
Green_4	-	58	3.55	60.19	14	57-71
Green_5	-	72	3.29	73.31	11	70-81
20% error	45.92-68.87	-	-	-	-	-
30% error	40.18-74.61	-	-	-	-	-
40% error	34.43-80.35	-	-	-	-	-
50% error	28.69-86.09	-	-	-	-	-

Table A-8. The summary table of 8th test analyzing the Hue value for 40 μl : 40 μl of cross-shape design

	Reference	Cross_40ul_test8				
		Mode	STD	AVG	Max-Min	Range
Blue	150.99	-	-	154.94	-	-
Yellow	35.36	-	-	38	-	-
Green_1	AVG: 57.39	38	8.87	45.64	25	37-62
Green_2	Range: 54-63	42	2.88	43.7	14	41-55
Green_3	-	45	3.16	46.43	12	44-56
Green_4	-	55	2.48	54.95	11.4	52.6-64
Green_5	-	61	3.87	60.04	13	56-69
20% error	45.92-68.87	-	-	-	-	-
30% error	40.18-74.61	-	-	-	-	-
40% error	34.43-80.35	-	-	-	-	-
50% error	28.69-86.09	-	-	-	-	-

Table A-9. The summary table of 9th test analyzing the Hue value for 40 μl : 40 μl of cross-shape design

	Reference	Cross_40ul_test9				
		Mode	STD	AVG	Max-Min	Range
Blue	150.99	-	-	150.31	-	-
Yellow	35.36	-	-	37.44	-	-
Green_1	AVG: 57.39	44	12.12	52.42	39	42-81
Green_2	Range: 54-63	49	4.01	52.66	17	49-66
Green_3	-	53	5.64	56.59	25	50-75
Green_4	-	61	6.23	63.89	25	59-84
Green_5	-	-	-	-	-	-
20% error	45.92-68.87	-	-	-	-	-
30% error	40.18-74.61	-	-	-	-	-
40% error	34.43-80.35	-	-	-	-	-
50% error	28.69-86.09	-	-	-	-	-

Table A-10. The summary table of 10th test analyzing the Hue value for 40 μl : 40 μl of cross-shape design

	Reference	Cross_40ul_test10				
		Mode	STD	AVG	Max-Min	Range
Blue	150.99	-	-	151.08	-	-
Yellow	35.36	-	-	36.7	-	-
Green_1	AVG: 57.39	44	11.73	52.93	57	42-99
Green_2	Range: 54-63	47	4.71	51.08	19	46-65
Green_3	-	47	4.62	50.07	17	46-63
Green_4	-	55	6.29	57.88	24	51-75
Green_5	-	63	6.26	67.14	21	62-83
20% error	45.92-68.87	-	-	-	-	-
30% error	40.18-74.61	-	-	-	-	-
40% error	34.43-80.35	-	-	-	-	-
50% error	28.69-86.09	-	-	-	-	-

APPENDIX B

Table of Frequency Distribution of Hue value of each test

Table B-1. The frequency distribution table of 1st test analyzing the Hue value for 40 μl : 40 μl of cross-shape design

Bin size	Range	Cross_40ul_test1				
		Green_1	Green_2	Green_3	Green_4	Green_5
42	0-42	0	0	0	0	0
52	43-52	40	40	0	0	0
64	53-64	23	23	32	32	32
74	65-74	8	8	71	71	71
84	75-84	4	4	24	24	24
94	85-94	6	6	0	0	0
104	95-104	10	10	0	0	0
114	105-114	16	16	0	0	0
124	115-124	12	12	0	0	0
134	125-134	5	2	0	0	0
Remaining		6	6	0	0	0
% of 53-64 range		18.54%	19.00%	25.19%	25.19%	25.19%
% By including 10% of error		54.61%	55.90%	81.10%	81.10%	81.10%

Table B-2. The frequency distribution table of 2nd test analyzing the Hue value for 40 μl : 40 μl of cross-shape design

Bin size	Range	Cross_40ul_test2				
		Green_1	Green_2	Green_3	Green_4	Green_5
42	0-42	2	0	1	0	0
52	43-52	54	24	7	0	0
64	53-64	10	44	85	56	0
74	65-74	2	28	22	36	0
84	75-84	2	20	6	29	77
94	85-94	4	15	0	0	36
104	95-104	6	0	0	0	8
114	105-114	4	0	0	0	0
124	115-124	0	0	0	0	0
134	125-134	20	0	0	0	0
Remaining		17	0	0	0	0
% of 53-64 range		9.61%	33.58%	70.24%	46.28%	0%
% By including 10% of error		54.54%	73.28%	94.21%	76.03%	0%

Table B-3. The frequency distribution table of 3rd test analyzing the Hue value for 40 μl : 40 μl of cross-shape design

Bin size	Range	Cross_40ul_test3				
		Green_1	Green_2	Green_3	Green_4	Green_5
42	0-42	0	0	0	0	0
52	43-52	51	67	77	0	0
64	53-64	10	20	14	93	0
74	65-74	6	16	19	17	110
84	75-84	4	7	0	0	0
94	85-94	10	0	0	0	0
104	95-104	14	0	0	0	0
114	105-114	8	0	0	0	0
124	115-124	6	0	0	0	0
134	125-134	1	0	0	0	0
Remaining		0	0	0	0	0
% of 53-64 range		9.09%	18.18%	12.72%	84.54%	0%
% By including 10% of error		60.90%	93.63%	100%	100%	100%

Table B-4. The frequency distribution table of 4th test analyzing the Hue value for 40 μl : 40 μl of cross-shape design

Bin size	Range	Cross_40ul_test4				
		Green_1	Green_2	Green_3	Green_4	Green_5
42	0-42	40	0	0	0	0
52	43-52	18	76	96	96	0
64	53-64	22	20	24	24	0
74	65-74	10	26	2	2	112
84	75-84	2	0	0	0	10
94	85-94	30	0	0	0	0
104	95-104	0	0	0	0	0
114	105-114	0	0	0	0	0
124	115-124	0	0	0	0	0
134	125-134	0	0	0	0	0
Remaining		0	0	0	0	0
% of 53-64 range		18.0327869%	16.3934426%	19.6721311%	19.6721311%	0%
% By including 10% of error		40.9836066%	100%	100%	100%	91.8032787%

Table B-5. The frequency distribution table of 5th est analyzing the Hue value for 40 μl : 40 μl of cross-shape design

Bin size	Range	Cross_40ul_test5				
		Green_1	Green_2	Green_3	Green_4	Green_5
42	0-42	34	0	0	0	0
52	43-52	38	108	86	0	96
64	53-64	6	14	36	58	24
74	65-74	10	0	0	58	2
84	75-84	0	0	6	6	0
94	85-94	6	0	0	0	0
104	95-104	22	0	0	0	0
114	105-114	6	0	0	0	0
124	115-124	0	0	0	0	0
134	125-134	0	0	0	0	0
Remaining		0	0	0	0	0
% of 53-64 range		4.91%	11.47%	28.12%	47.54%	19.67%
% By including 10% of error		44.26%	100%	95.31%	95.08%	100%

Table B-6. The frequency distribution table of 6th test analyzing the Hue value for 40 μl : 40 μl of cross-shape design

Bin size	Range	Cross_40ul_test6				
		Green_1	Green_2	Green_3	Green_4	Green_5
42	0-42	32	36	0	0	0
52	43-52	34	34	82	0	0
64	53-64	6	6	39	100	0
74	65-74	26	26	0	21	56
84	75-84	2	2	0	0	23
94	85-94	16	16	0	0	0
104	95-104	1	1	0	0	0
114	105-114	0	0	0	0	0
124	115-124	0	0	0	0	0
134	125-134	0	0	0	0	0
Remaining		0	0	0	0	0
% of 53-64 range		5.12%	4.95%	32.23%	82.64%	0%
% By including 10% of error		56.41%	54.54%	100%	100%	70.88%

Table B-7. The frequency distribution table of 7th test analyzing the Hue value for 40 μl : 40 μl of cross-shape design

Bin size	Range	Cross_40ul_test7				
		Green_1	Green_2	Green_3	Green_4	Green_5
42	0-42	32	36	0	0	0
52	43-52	34	34	82	0	0
64	53-64	6	6	39	100	0
74	65-74	26	26	0	21	56
84	75-84	2	2	0	0	23
94	85-94	16	16	0	0	0
104	95-104	1	1	0	0	0
114	105-114	0	0	0	0	0
124	115-124	0	0	0	0	0
134	125-134	0	0	0	0	0
Remaining		0	0	0	0	0
% of 53-64 range		5.12%	4.95%	32.23%	82.64%	0%
% By including 10% of error		56.41%	54.54%	100%	100%	70.88%

Table B-8. The frequency distribution table of 8th test analyzing the Hue value for 40 μl : 40 μl of cross-shape design

Bin size	Range	Cross_40ul_test8				
		Green_1	Green_2	Green_3	Green_4	Green_5
42	0-42	66	52	0	0	0
52	43-52	20	68	109	0	0
64	53-64	35	1	12	121	99
74	65-74	0	0	0	0	22
84	75-84	0	0	0	0	0
94	85-94	0	0	0	0	0
104	95-104	0	0	0	0	0
114	105-114	0	0	0	0	0
124	115-124	0	0	0	0	0
134	125-134	0	0	0	0	0
Remaining		0	0	0	0	0
% of 53-64 range		28.92%	0.82%	9.91%	100%	81.81%
% By including 10% of error		45.45%	57.02%	100%	100%	100%

Table B-9. The frequency distribution table of 9th test analyzing the Hue value for 40 μl : 40 μl of cross-shape design

Bin size	Range	Cross_40ul_test9			
		Green_1	Green_2	Green_3	Green_4
42	0-42	6	0	0	0
52	43-52	78	72	22	0
64	53-64	12	48	85	89
74	65-74	8	1	13	20
84	75-84	17	0	1	12
94	85-94	0	0	0	0
104	95-104	0	0	0	0
114	105-114	0	0	0	0
124	115-124	0	0	0	0
134	125-134	0	0	0	0
Remaining		0	0	0	0
% of 53-64 range		9.91%	39.66%	70.24%	73.55%
% By including 10% of error		80.99%	100%	99.17%	90.08%

Table B-10. The frequency distribution table of 10th test analyzing the Hue value for 40 μl : 40 μl of cross-shape design

Bin size	Range	Cross_40ul_test10				
		Green_1	Green_2	Green_3	Green_4	Green_5
42	0-42	8	0	0	0	0
52	43-52	68	68	92	22	0
64	53-64	20	50	29	76	56
74	65-74	16	3	0	22	43
84	75-84	8	0	0	1	22
94	85-94	0	0	0	0	0
104	95-104	1	0	0	0	0
114	105-114	0	0	0	0	0
124	115-124	0	0	0	0	0
134	125-134	0	0	0	0	0
Remaining		0	0	0	0	0
% of 53-64 range		16.52%	41.32%	23.96%	62.80%	46.28%
% By including 10% of error		85.95%	100%	100%	99.17%	81.81%